THE ASTRONOMICAL JOURNAL VOLUME 100, NUMBER 4 OCTOBER 1990

WHERE DOES THE DISK STOP AND THE HALO BEGIN? KINEMATICS IN A ROTATION FIELD

HEATHER L. MORRISON,[a] CHRIS FLYNN,[b] AND K. C. FREEMAN
Mount Stromlo and Siding Spring Observatories, Institute of Advanced Studies, The Australian National University, Private Bag, Woden P. O. ACT 2606, Australia

Received 31 October 1989; revised 20 February 1990

ABSTRACT

A sample of G and K giants approximately 4 kpc from the Sun, covering the abundance range from solar to extreme halo has been selected without kinematic bias in a field aligned to measure galactic rotation. Accurate abundances, distances, and radial velocities have been measured. This sample has been combined with nonkinematically selected solar neighborhood objects taken from the literature, in order to examine the kinematics of the transition from disk to "thick disk" to halo. The metal-rich objects in the sample, with $0 > [\mathrm{Fe/H}] > -0.8$, rotate rapidly around the galactic center and have low azimuthal velocity dispersion, $\sigma_\phi = 40 \pm 10$ km s^{-1}. For objects in the range $-0.5 > [\mathrm{Fe/H}] > -0.8$, we find a small value for the asymmetric drift of 35 ± 10 km s^{-1}. We associate these objects with the thick disk, confirming the kinematical results of Ratnatunga and Freeman (1989) and others. In the abundance range $-1.0 \geqslant [\mathrm{Fe/H}] \geqslant -1.6$ we find, in addition to objects with normal halo kinematics, objects in a disk configuration, confirming the results of Norris, Bessell, and Pickles (1985). This disk is rotating rapidly, $V_{\mathrm{rot}} = 170 \pm 15$ km s^{-1}, and has a scale height of 1.4 ± 0.7 kpc—these kinematical and spatial properties are similar to those of the thick disk. We show that these objects have different kinematics from that of the globular clusters and a sample of local RR Lyraes in the same abundance range. This suggests to us that these objects are better associated with the thick disk than the halo, and we refer to them as "metal-weak thick-disk stars." Hence we suggest that the conventional chemical description of the thick disk (Gilmore and Wyse 1985) be widened to include stars with abundances as low as $[\mathrm{Fe/H}] = -1.6$. At the galactic plane, the density of these metal-weak thick-disk stars is similar to that of halo stars, so they significantly affect the measurement, from samples selected on abundance, of the components of the velocity ellipsoid for the halo in the solar neighborhood. For the halo giants in our sample we measure $\sigma_\phi = 102 \pm 24$ and $V_{\mathrm{rot}} = 17 \pm 24$ km s^{-1}. The rotation velocity and velocity ellipsoid for the metal-weak halo in the solar neighborhood have been rederived for objects with $[\mathrm{Fe/H}] \leqslant -1.6$ from the large sample of Norris (1986), thus removing the possibility of contamination by metal-weak thick-disk stars. We derive $V_{\mathrm{rot}} = 25 \pm 15$ km s^{-1} and $(\sigma_r, \sigma_\phi, \sigma_\theta) = (133 \pm 8, 98 \pm 13, 94 \pm 6)$ km s^{-1}. These values are more consistent with other information about the shape of the halo.

I. INTRODUCTION

The study of the stellar populations which make up our galaxy yields important clues with which to reconstruct its history. Recently, great improvements in observational techniques have made available large samples of objects with accurate kinematic, abundance and/or age data. The size of these samples is leading towards better descriptions of the Galaxy's stellar populations in terms of chemistry, kinematics, age, and space distributions. In addition, we can begin to examine how clearly the various boundaries between populations should be drawn.

In this paper, we have obtained a sample of G and K giants with abundances covering the full range from disk to halo, in a field chosen to measure rotational kinematics. This study of the disk to halo transition will involve three of the Galaxy's populations: the disk, the "thick disk," and the halo. Of these, the thick disk is the most controversial. It was introduced by Gilmore and Reid (1983), but opinions are still divided about its existence as a separate population, and also, to some extent, its properties. For a recent summary of work in this area, see Freeman (1987).

In this paper, our use of "thick disk" means a set of stars with the particular kinematics outlined by Freeman (1987): i.e., an asymmetric drift of about 30 km s^{-1} and velocity dispersion components that are about twice those of the old disk. Our aim in this work is to identify the range of stellar abundances that are consistent with this kinematical definition, so our use of thick disk does not have the conventional (see Gilmore and Wyse 1985) chemical connotations.

Before we consider the thick disk, we should review briefly the two other populations—the old disk and the halo. The old disk is the best understood of the three. It is kinematically cold and rotationally supported, and is represented in the solar neighborhood by the bulk of the metal-rich stars. Halo stars are metal-weak, very rare in the solar neighborhood, and form a slowly rotating, high velocity dispersion population.

Once the basic properties of the major components have been established, there are further questions: for example, are the populations distinct and well separated or is there an overlap between the populations, in abundance, kinematics, or age? In particular, is there an abrupt change from disk to halo, or a region of transition between them?

The thick disk itself certainly has transitional properties. It has an intermediate scale height (about 1 kpc), and its rotation is rapid (but less rapid than the old, metal-rich thin disk). The components of its velocity dispersion are about twice those of the old disk.

Several studies (i.e., Gilmore and Wyse 1985; Carney, Latham, and Laird 1989) have proposed that the thick-disk

---

[a] Current address: Observatories of the Carnegie Insitution of Washington, 813 Santa Barbara St., Pasadena, CA 91101.

[b] Current address: Astronomisches Rechen Institut, Mönchofstrasse 12-14, D-6900 Heidelberg 1, Federal Republic of Germany.

*Defined in the usual way by $[\mathrm{Fe/H}] = \log(\mathrm{Fe/H})_\star - \log(\mathrm{Fe/H})_\odot$.

stars have abundances intermediate between disk and halo. In this conventional description of the thick disk, Gilmore and Wyse (1985) suggested that the peak of its abundance distribution is at [Fe/H]* ≈ -0.6 with a spread in abundance of about $\sigma_{[\mathrm{Fe/H}]} \approx 0.3$. However, Norris, Bessell, and Pickles (1985—hereafter referred to as NBP), have found stars in the solar neighborhood which have [Fe/H] < -1, and are on low eccentricity, high angular momentum orbits, with z velocity dispersion similar to that of the thick disk and suggested that these stars are the *metal-weak tail* of the thick disk. The kinematics of these metal-weak thick-disk stars are so different from those of the classical metal-weak halo, that there is little difficulty in distinguishing between them. However, distinguishing between stars of the thin and thick disks is more difficult, if they are indeed separate populations. The suggested kinematical and abundance parameters of the thick disk are relatively close to those of the thin disk, making it difficult to decide whether they are separate populations on kinematical and chemical grounds alone. Stars with an abundance [Fe/H] ≈ -0.5 in the solar neighborhood show clear signs of higher velocity dispersion and asymmetric drift relative to the more metal-rich stars: Do they belong to the thick or the thin disk, or are the two populations really one, with a somewhat larger range of kinematic properties, as suggested by Norris (1987)?

We aim in this paper to define more clearly the concepts of thick disk and halo, by examining the disk to halo transition from objects that cover the full disk to halo range of abundance. We also aim to identify stars with properties consistent with the thick-disk definitions above. A better understanding of the nature of the overlap of the thick disk with the halo will help us improve the kinematic parameters for genuine halo stars (uncontaminated by thick-disk stars). We do not intend to address directly questions about the place of the thick disk in galactic formation and evolution. For example, were the thick disk stars formed in a single well-defined event, or do the somewhat hotter kinematics of the metal-weaker stars of the disk simply result from the secular evolution of the disk as a whole? We leave the question of the origin of the thick disk open, and use the term thick disk without implying the existence of a cosmogonically separate population.

A powerful way to study the possible overlap between disk and halo is to utilize simultaneously *both* of the kinematical differences between the disk and halo: The difference in galactocentric rotational velocity and in velocity dispersion. This can be done from radial velocities alone by studying the velocity distribution at a position in the Galaxy where the line-of-sight velocity is dominated by the rotational component. Such a distribution will show the clearest separation between disk and halo, and thus display the greatest sensitivity to objects with intermediate properties.

For this work, it is essential to have nonkinematically selected samples. Since the Sun has a near-circular orbit, surveys of high proper-motion stars have a "blind spot" with respect to other stars with roughly circular orbits; it is very difficult to derive an unbiased estimate of how many stars have similar motion to the Sun from such surveys.

So, a study of the transition from disk to halo, using galactocentric rotation and velocity dispersion as discriminants, requires: (a) objects which are selected without kinematic bias, and (b) objects which are found in the disk, thick disk, and halo: that is, with abundances ranging from mildly to extremely metal deficient.

We have chosen to study G and K giants, because they can be found with a range of [Fe/H] from above solar to very metal weak, and we have identified them from an objective prism survey. The giants were found in two fields, chosen so that the measured radial velocity is dominated by the rotational component. Their z heights range from 200 pc to 6 kpc; they are about 8 kpc from the galactic center, and roughly 4 kpc away from the Sun. We have determined accurate abundances and luminosities for these stars using DDO photometry, and measured the radial velocity for each star. Because this sample of giants is at a similar galactocentric radius to the Sun, we have combined it with similar samples of stars in the solar neighborhood, thus gaining a sample of almost 200 giants.

From these data, we have estimated the mean rotational velocity (V_{rot}) and velocity dispersion in the azimuthal direction (σ_ϕ) for the disk and halo, and investigated the transition in abundance and kinematics between these populations. The metal-rich giants ([Fe/H] > -0.5) have kinematic properties consistent with previous measures for the old disk.

We have found stars of lower abundance, whose kinematic properties are consistent with membership of the thick disk, and whose abundance distribution shows a large overlap with the abundance distribution of the halo, in a region extending down to [Fe/H] $= -1.6$. We have derived population parameters (scale height, V_{rot}, and normalization in the plane) for the stars in this overlap region. We confirm that there are stars with abundances ranging as low as [Fe/H] $= -1.6$ which form the metal-weak tail of the thick disk, as originally suggested by NBP. Two independent kinematically derived estimates of the scale length of the thick disk suggest that it is slightly shorter than the scale length of the old disk.

These results lead us to suggest that the conventional chemical description of the thick disk be widened to include some stars with abundances as low as [Fe/H] $= -1.6$. We therefore conclude that it is necessary to use both abundance *and* kinematics to define membership of the halo, for stars with [Fe/H] $\geqslant -1.6$ within several kpc of the galactic plane, as neither is adequate on its own. We derive improved kinematical parameters for the halo, which are more consistent with other information about its shape.

In Secs. II, III, and IV we describe selection of candidates, observations and the derivation of abundances, distances, and reddenings. In Sec. V we describe our extension of the Frenk and White (1980) method of measuring V_{rot} to estimation of velocity dispersion. In Sec. VI our data are presented and we conclude that the disk and halo abundance distributions overlap but their kinematics are discontinuous. Our sample is combined with solar neighborhood giants from the literature in Sec. VII. This sample confirms and extends our earlier results. In Sec. VIII we compare the kinematics of the metal-weak red giants with kinematics of halo objects (the globular clusters and local RR Lyraes), present evidence for thick-disk abundances extending as low as [Fe/H] $= -1.6$, and discuss the implications of our results for definitions of the thick disk, for halo kinematics, and for theories of galaxy formation. Our conclusions are in Sec. IX.

II. SELECTION OF GIANT CANDIDATES

a) The PHI and 959 Fields

The G and K giants offer several advantages: they are bright and very numerous, their photometric parallaxes can be accurately determined from DDO photometry, their radial velocities are easily measured, and they cover the whole range in abundance from disk to extreme halo.

To measure rotation most directly from line-of-sight velocities, two fields were chosen at $l = 300°$, $b = +30°$ (the PHI field) and at $l = 60°$, $b = -30°$ (UK Schmidt field 959). Objects about 4 kpc along these lines of sight are close to the "tangent point" where their radial velocities are perpendicular to their galactocentric radius vector and are hence dominated by the rotational component of their space velocities. We set out to locate late-type giants close to this position along the lines of sight. Choosing a target absolute magnitude $M_V = -1.0$ and the magnitude range $V = 10.5$ to 13.5 centered our survey on the tangent point. This magnitude range optimized the survey for the discovery of halo objects. The more metal-strong objects found were on average 2 kpc closer than the tangent point.

We briefly describe here our selection of halo giant candidates redder than $B - V = 0.7$, and disk giant candidates redder than $B - V = 1.0$ from direct and prism plates. These color cutoffs were chosen since the giant branch moves blueward for decreasing metallicity. Our luminosity classifications come from DDO photometry, which is not calibrated for metal-weak stars with $B - V \lesssim 0.7$. The disk giant color cutoff was chosen to avoid subgiants. Complete details are in Flynn and Morrison (1990).

For the PHI field, three objective prism plates with matching B and R direct plates were taken with the Uppsala Schmidt telescope at Siding Spring Observatory. For the 959 field, one prism and matching B and R direct plates were taken by the staff of the UK Schmidt Telescope Unit. The total sky coverage of the two regions was 40.0° sq. Photographic $B - R$ colors were obtained from the direct plates and the prism images of stars in the appropriate color range scanned with the MSO PDS. The prism spectra extended from about 3500 Å to the cutoff of the IIIa-J emulsion at about 5400 Å. For late-type stars this includes Ca II H and K, the blue and violet CN bands, the G band, Hβ, and Mgb + MgH. A wavelength calibration of the prism dispersion was determined relative to the emulsion cutoff as a reference point.

The strength of the stellar Ca II H and K lines (measured from the PDS scans) as a function of $B - R$ color was used to identify giant candidates more metal weak than $[\mathrm{Fe/H}] \approx -1$. The technique was extended to the discovery of giants more metal strong than $[\mathrm{Fe/H}] \approx -1$ and with $B - V > 1.0$ by use of the blue and violet CN bands. The MgH feature at 5200 Å and the blend of Mg I and Fe I lines between 3816 and 3841 Å were used to remove the very large numbers of foreground dwarfs. Approximately 160 candidate giants were selected from the two regions for photoelectric and spectroscopic observations.

b) The Gpec Stars

The catalog of Stock (1984) lists objective prism radial velocities, spectral types and photographic magnitudes from $m_{\mathrm{pg}} \approx 9.0$ to $m_{\mathrm{pg}} \approx 12.0$ in a 300° sq. area which partially overlaps our PHI region. Stock *et al.* (1984) found from slit spectra that stars classified as "Gpec" in the Stock catalog were in general "mid G to early K in type and moderately to extremely weak in metals."

We used these Gpec stars to supplement our survey; 35 stars which roughly overlapped our survey region were chosen from Stock (1984). *BV* photometry was obtained with the Siding Spring 0.6 m telescope and 16 stars redder than $B - V = 0.70$ (the color cutoff of our survey) were placed on our list of giant candidates. These stars have been selected using the Gpec classification only; the objective-prism radial velocities were not used.

There was effectively no overlap between the Stock survey and our PHI fields: the Stock survey (of Gpec stars) covered a larger area, but had brighter magnitude limits, than the PHI fields. There was a small overlap in magnitude between the faint end of the Stock survey and the bright end of the PHI survey. None of the giants discovered from the Stock survey was both in the magnitude range of the PHI fields and in areas covered by the PHI plates. We discovered one metal-weak star in the overlap area which was not identified in the Stock survey. However, this star is at the faint end of the Stock magnitude range ($V = 11.9$) where Stock does not claim completeness over his entire survey area.

III. OBSERVATIONS

a) DDO Photometry

We chose the intermediate band DDO photometric system of McClure (1976) in order to remove dwarf stars from the sample and to measure accurate abundances and luminosities of the giants.

DDO measurements for all the candidate giants were made during the period 1986–1988, using a standard filter set and a GaAs photomultiplier mounted on the 2.3 m telescope at Siding Spring Observatory. On average 18 stars were observed each night from the lists of McClure and Forrester (1981) and NBP, in order to transform the observations to the standard DDO system. The Spider package (written by A. C. Cameron and modified by E. M. Green) was used to reduce our photometric data. It allows the simultaneous estimation of instrumental transformations and extinction coefficients. Standard errors for a single measurement, derived from multiple observations of program stars in the colors C4548, C4245, C4142, C3842 were 0.009, 0.013, 0.013, and 0.017, respectively.

In Table I we show the name, luminosity class (determined from DDO photometry as described in Appendix A), coordinates, and DDO colors for each star. The number of DDO measurements N_D is shown in the final column.

b) Broadband Photometry

BV photometry was obtained for the giants during 1987 and 1988 with the 1.0 and 2.3 m telescopes at Siding Spring, using a GaAs photomultiplier. Standards were selected from the compilation of Cousins standards by Menzies, Banfield, and Laing (1980); Landolt (1983), Bessell (1988), and Graham (1982). Using stars with multiple observations, we derive standard errors for a single measurement of 0.015 in V and 0.013 in $B - V$. The V and $B - V$ data for the giants are shown in columns 2 and 3 of Table II.

c) Radial Velocities

Spectra for our giants and several of the dwarfs were obtained with the Mount Stromlo 1.9 m telescope using the Cassegrain spectrograph and the Photon Counting Array (Stapinski *et al.* 1981) during 1986 and 1987. We sampled about 400 Å around the Mgb + MgH feature using a dispersion of 50 Å/mm (35 km s^{-1} channel^{-1}). Radial-velocity

TABLE I. DDO photometry.

Name	Lum	α (1950) δ		C4548	C4245	C4142	C3842	N_D
959 11 2	III	21 23 22.1	+07 18 51	1.278	0.987	0.123	−0.248	1
959 11 3	III	21 24 17.1	+07 16 23	1.172	0.805	0.061	−0.547	2
959 11 13	III	21 22 43.8	+07 10 57	1.145	0.757	0.040	−0.613	1
959 11 36	III	21 21 00.6	+06 55 22	1.193	0.835	0.118	−0.464	1
959 11 39	III	21 24 01.5	+06 52 48	1.193	0.843	0.098	−0.437	1
959 11 51	III	21 22 40.3	+06 43 31	1.180	0.822	0.049	−0.535	1
959 11 58	III	21 21 30.2	+06 38 54	1.138	0.751	0.024	−0.648	2
959 11 59	V	21 20 56.5	+06 38 27	1.057	0.744	0.008	−0.657	1
959 11 78	V	21 22 28.5	+06 28 34	1.008	0.605	0.018	−0.793	1
959 11 81	III/IV	21 22 54.0	+06 22 14	1.187	0.912	0.128	−0.327	1
959 11 94	III	21 21 14.2	+06 09 12	1.140	0.702	0.040	−0.664	3
959 11 118	V	21 22 37.4	+05 50 41	1.041	0.690	0.003	−0.755	1
959 11 142	III/IV	21 22 11.4	+05 33 12	1.141	0.758	0.057	−0.642	2
959 11 163	III	21 23 12.9	+05 16 49	1.347	0.987	0.161	−0.086	1
959 12 24	III/IV	21 28 45.6	+06 59 38	1.159	0.889	0.150	−0.376	1
959 12 44	III	21 25 26.8	+06 33 23	1.114	0.648	0.032	−0.776	2
959 12 70	V	21 28 49.6	+06 03 25	1.064	0.801	0.099	−0.508	1
959 12 116	III/IV	21 25 43.4	+05 31 20	1.198	0.883	0.156	−0.321	2
959 12 121	V	21 26 05.2	+05 27 13	1.039	0.608	0.055	−0.725	1
959 12 126	III/IV	21 26 52.2	+05 23 54	1.204	0.898	0.149	−0.356	2
959 31 13	IV/V	21 22 45.5	+04 54 34	1.089	0.759	0.025	−0.617	2
959 31 22	V	21 22 32.1	+04 48 31	1.039	0.690	0.013	−0.726	1
959 31 43	V	21 23 32.7	+04 38 01	1.106	0.966	0.008	−0.452	1
959 31 52	V	21 24 22.2	+04 33 55	1.069	0.749	0.017	−0.630	1
959 31 59	III/IV	21 21 59.4	+04 30 26	1.169	0.852	0.149	−0.419	2
959 31 66	III/IV	21 22 23.6	+04 26 49	1.119	0.778	0.032	−0.605	1
959 31 77	III/IV	21 23 44.3	+04 17 33	1.200	0.874	0.139	−0.354	1
959 31 79	IV	21 21 26.9	+04 15 35	1.089	0.768	0.035	−0.582	1
959 31 87	III	21 21 26.7	+04 10 57	1.129	0.714	0.028	−0.700	1
959 31 108	III	21 19 58.3	+04 01 23	1.167	0.832	0.056	−0.498	2
959 31 119	V	21 20 14.7	+03 54 10	1.046	0.686	0.047	−0.653	1
959 31 129	IV	21 23 24.8	+03 48 16	1.078	0.719	0.001	−0.747	3
959 31 167	III	21 22 25.5	+03 29 49	1.194	0.737	0.047	−0.659	1
959 31 170	V	21 21 26.7	+03 27 38	1.062	0.784	−0.018	−0.635	1
959 31 176	III/IV	21 22 52.8	+03 21 49	1.156	0.819	0.091	−0.514	2
959 31 190	III/IV	21 23 24.1	+03 14 35	1.341	1.167	0.206	0.066	1
959 32 12	III/IV	21 25 30.5	+04 53 30	1.204	0.890	0.116	−0.359	1
959 32 13	IV	21 25 22.7	+04 52 45	1.104	0.767	0.040	−0.583	1
959 32 20	V	21 27 50.3	+04 48 18	1.030	0.672	0.031	−0.673	1
959 32 22	III/IV	21 28 20.6	+04 47 35	1.194	0.854	0.143	−0.397	1
959 32 28	V	21 27 34.0	+04 43 52	1.066	0.726	0.051	−0.586	1
959 32 32	III/IV	21 27 30.3	+04 41 43	1.208	0.923	0.144	−0.239	1
959 32 43	III/IV	21 28 13.4	+04 34 58	1.298	1.133	0.268	0.015	2
959 32 59	III	21 28 03.9	+04 23 04	1.239	0.881	0.118	−0.338	2
959 32 69	III/IV	21 25 14.6	+04 17 42	1.194	0.925	0.131	−0.315	2
959 32 77	V	21 24 33.3	+04 08 23	1.035	0.693	−0.006	−0.767	1
959 32 78	III/IV	21 25 11.5	+04 07 03	1.167	0.874	0.097	−0.371	1
959 32 87	III	21 26 01.4	+04 00 56	1.328	0.944	0.126	−0.180	1
959 32 98	III	21 26 15.5	+03 56 04	1.145	0.736	0.015	−0.672	1
959 32 108	III	21 28 50.0	+03 52 43	1.216	0.819	0.110	−0.374	1

TABLE I. (continued)

Name	Lum	α (1950)	δ	C4548	C4245	C4142	C3842	N_D
959 32 132	IV	21 25 43.4	+03 41 30	1.126	0.753	0.063	−0.563	1
959 32 144	III/IV	21 27 00.5	+03 32 08	1.227	0.973	0.150	−0.230	1
959 32 154	III/IV	21 25 55.0	+03 25 20	1.179	0.858	0.089	−0.437	2
959 32 156	V	21 26 05.4	+03 24 46	1.062	0.747	−0.014	−0.720	1
959 32 162	III/IV	21 23 54.0	+03 32 41	1.265	1.045	0.308	−0.066	1
959 32 167	V	21 27 24.3	+03 14 57	1.040	0.624	0.055	−0.626	1
959 32 168	V	21 25 48.6	+03 14 49	1.009	0.581	0.017	−0.826	1
959 32 184	III	21 24 33.7	+02 57 50	1.207	0.869	0.140	−0.319	2
959 32 190	III/IV	21 25 19.3	+02 54 08	1.182	0.844	0.078	−0.445	1
959 41 39	III/IV	21 10 16.0	+03 07 36	1.188	0.860	0.115	−0.372	1
959 41 128	III/IV	21 10 34.6	+04 13 22	1.214	0.896	0.167	−0.304	1
959 41 150	III/IV	21 11 27.6	+04 32 19	1.182	0.820	0.103	−0.455	1
959 41 175	III/IV	21 14 18.1	+04 46 55	1.207	0.882	0.146	−0.336	1
959 42 2	III	21 18 02.6	+02 35 09	1.165	0.720	0.028	−0.667	1
959 42 26	III/IV	21 18 12.2	+02 44 47	1.250	1.019	0.160	−0.179	1
959 42 49	III/IV	21 18 02.0	+03 04 16	1.179	0.848	0.043	−0.517	1
959 42 51	V	21 19 25.1	+03 04 51	1.073	0.747	0.088	−0.617	1
959 42 72	III	21 18 07.6	+03 16 11	1.216	0.730	0.070	−0.561	1
959 42 74	IV/V	21 18 38.2	+03 17 19	1.076	0.657	0.026	−0.801	1
959 42 78	III/IV	21 19 41.1	+03 19 38	1.184	0.832	0.115	−0.424	1
959 42 99	III	21 16 33.6	+03 40 19	1.274	1.003	0.187	−0.125	1
959 42 121	IV	21 17 26.0	+03 57 07	1.133	0.868	0.070	−0.483	1
959 42 125	III/IV	21 17 34.5	+04 00 18	1.281	1.071	0.275	0.016	1
959 42 134	III	21 15 43.5	+04 05 23	1.213	0.862	0.022	−0.570	1
959 42 158	IV/V	21 17 50.7	+04 26 21	1.068	0.686	0.033	−0.693	1
959 42 186	III/IV	21 17 55.0	+04 49 04	1.190	0.893	0.095	−0.419	1
GPEC 106	III	11 52 21.0	−26 00 30	1.120	0.629	0.019	−0.925	1
GPEC 465	III/IV	12 05 06.0	−29 47 39	1.117	0.808	0.035	−0.543	2
GPEC 515	III	12 06 44.0	−29 15 50	1.255	0.774	0.094	−0.486	1
GPEC 1172	III	12 30 57.0	−34 16 45	1.094	0.548	0.063	−0.822	2
GPEC 1206	III	12 31 29.0	−34 37 10	1.187	0.617	0.079	−0.735	2
GPEC 1434	III/IV	12 35 00.0	−34 46 31	1.186	0.885	0.145	−0.388	2
GPEC 1834	III	12 41 02.0	−32 47 16	1.116	0.717	0.016	−0.693	3
GPEC 1940	IV/V	12 42 46.0	−30 28 21	1.062	0.661	−0.012	−0.852	2
GPEC 2045	III	12 44 42.0	−28 06 36	1.180	0.746	0.035	−0.675	1
GPEC 2156	III	12 46 16.0	−34 02 06	1.152	0.785	0.092	−0.523	1
GPEC 2193	V	12 46 48.0	−33 53 09	1.127	1.181	0.003	−0.364	1
GPEC 2643	III	12 59 15.0	−32 53 03	1.354	0.834	0.154	−0.307	6
GPEC 2650	III	12 59 32.0	−34 05 26	1.166	0.633	0.070	−0.714	5
GPEC 2904	III	13 07 26.0	−33 26 39	1.255	0.732	0.115	−0.482	2
GPEC 3038	III	13 10 51.0	−31 39 30	1.140	0.721	0.004	−0.755	1
GPEC 3672	III	13 26 05.0	−31 05 12	1.130	0.726	0.034	−0.630	2
PHI2/1 43	III	12 26 55.7	−32 16 33	1.179	0.733	0.054	−0.629	2
PHI2/1 49	III/IV	12 25 32.7	−31 26 47	1.211	0.940	0.122	−0.355	1
PHI2/1 52	III	12 25 08.4	−31 58 35	1.145	0.625	0.064	−0.803	1
PHI2/1 66	III	12 23 08.3	−31 52 34	1.131	0.695	0.030	−0.680	1
PHI2/1 69	III	12 22 48.1	−31 23 44	1.180	0.835	0.115	−0.396	1
PHI2/2 2	III	12 22 41.4	−31 28 41	1.267	1.045	0.294	−0.096	1
PHI2/2 4	III	12 22 10.4	−32 09 48	1.242	0.936	0.098	−0.325	1
PHI2/2 6	V	12 22 05.2	−32 20 18	1.059	0.661	−0.014	−0.825	1
PHI2/2 7	III	12 21 59.7	−31 37 39	1.214	0.807	0.069	−0.502	1

TABLE I. (continued)

Name	Lum	α (1950)	δ	C4548	C4245	C4142	C3842	N_D
PHI2/2 8	III/IV	12 21 36.7	−31 32 55	1.200	0.913	0.108	−0.407	2
PHI2/2 10	III/IV	12 21 32.8	−32 05 50	1.223	0.951	0.178	−0.234	1
PHI2/2 19	III/IV	12 33 30.4	−30 46 45	1.182	0.861	0.124	−0.402	1
PHI2/2 23	III	12 33 13.8	−30 51 30	1.182	0.630	0.083	−0.733	1
PHI2/2 31	III/IV	12 32 20.6	−31 09 20	1.222	0.959	0.106	−0.251	1
PHI2/2 33	III/IV	12 32 02.6	−30 44 28	1.191	0.876	0.129	−0.383	1
PHI2/2 40	III	12 30 52.9	−30 41 21	1.178	0.838	0.072	−0.464	3
PHI2/2 46	III	12 29 55.0	−31 15 54	1.400	1.007	0.154	−0.023	2
PHI2/2 49	III	12 29 28.6	−30 00 02	1.208	0.864	0.060	−0.483	1
PHI2/2 69	IV	12 27 30.8	−30 33 05	1.138	0.879	0.128	−0.411	1
PHI2/2 71	III/IV	12 29 19.0	−30 31 45	1.186	0.872	0.128	−0.396	1
PHI2/2 73	IV	12 27 19.3	−30 59 00	1.138	0.912	0.110	−0.370	1
PHI2/2 74	III/IV	12 27 12.0	−30 23 41	1.202	0.869	0.144	−0.391	2
PHI2/2 97	III	12 25 02.4	−30 48 22	1.163	0.733	0.079	−0.529	1
PHI2/2 98	V	12 25 03.7	−31 05 30	1.059	0.797	0.037	−0.624	1
PHI2/2 100	III	12 26 37.0	−30 34 46	1.172	0.809	0.064	−0.546	3
PHI2/2 102	V	12 24 33.9	−30 22 06	1.043	0.662	0.018	−0.699	1
PHI2/2 111	III/IV	12 25 32.0	−30 34 00	1.096	0.752	0.063	−0.636	2
PHI2/2 113	IV/V	12 23 20.1	−31 04 44	1.075	0.758	0.019	−0.618	1
PHI2/2 121	III/IV	12 22 40.2	−31 19 59	1.102	0.799	0.028	−0.563	1
PHI2/2 127	V	12 22 05.1	−30 43 47	1.054	0.599	−0.003	−0.863	1
PHI2/2 132	V	12 21 26.0	−30 08 33	1.052	0.652	0.041	−0.699	1
PHI4/1 6	V	12 49 43.7	−30 25 15	1.058	0.717	0.024	−0.670	1
PHI4/1 7	III	12 49 34.8	−29 45 37	1.342	1.007	0.166	−0.103	2
PHI4/1 19	III/IV	12 49 05.4	−30 43 05	1.156	0.834	0.073	−0.503	3
PHI4/1 21	III	12 49 01.0	−30 29 42	1.132	0.672	0.031	−0.814	1
PHI4/1 33	V	12 48 12.4	−30 55 27	1.134	0.924	0.093	−0.378	1
PHI4/1 58	V	12 46 45.6	−30 32 36	0.992	0.596	0.015	−0.856	1
PHI4/1 60	IV/V	12 46 43.0	−30 45 19	1.077	0.738	0.000	−0.726	1
PHI4/1 62	III	12 46 42.8	−30 57 38	1.194	0.844	0.056	−0.457	1
PHI4/1 63	III	12 46 38.1	−30 41 46	1.155	0.738	0.055	−0.593	6
PHI4/1 65	III	12 46 25.0	−30 58 07	1.109	0.732	−0.001	−0.745	1
PHI4/1 67	V	12 46 13.5	−30 14 46	1.032	0.629	0.029	−0.738	1
PHI4/1 99	III	12 44 36.4	−30 25 11	1.311	0.805	0.134	−0.390	3
PHI4/1 106	V	12 44 22.0	−31 02 08	1.008	0.597	0.007	−0.827	1
PHI4/1 153	V	12 42 30.9	−30 47 33	1.023	0.629	−0.016	−0.822	1
PHI4/1 164	IV:	12 41 56.1	−31 02 50	1.110	0.747	−0.019	−0.661	1
PHI4/1 167	III	12 41 39.2	−29 38 55	1.259	0.803	0.056	−0.460	2
PHI4/1 170	III	12 41 27.5	−29 45 23	1.225	0.813	0.063	−0.479	2
PHI4/1 176	III	12 41 23.0	−30 21 55	1.164	0.787	0.025	−0.595	2
PHI4/1 177	V	12 41 31.0	−31 03 28	1.006	0.544	0.042	−0.789	2
PHI4/1 178	III/IV	12 41 14.8	−29 38 09	1.152	0.792	0.044	−0.553	1
PHI4/1 180	V	12 41 15.0	−30 40 14	1.105	0.817	0.005	−0.573	1
PHI4/2 1	V	12 40 27.0	−29 45 53	1.078	0.791	0.049	−0.575	1
PHI4/2 15	III/IV	12 36 45.2	−29 38 42	1.181	0.859	0.102	−0.375	1
PHI4/2 20	III/IV	12 36 42.3	−30 23 27	1.142	0.809	0.095	−0.512	1
PHI4/2 33	III/IV	12 48 11.2	−30 55 18	1.151	0.906	0.106	−0.350	1
PHI4/2 34	III	12 35 49.3	−29 36 37	1.147	0.792	0.029	−0.649	2
PHI4/2 35	III	12 35 45.4	−29 43 40	1.142	0.720	0.041	−0.662	2
PHI4/2 37	V	12 35 39.7	−30 26 40	1.088	0.854	0.056	−0.485	1
PHI4/2 47	V	12 34 56.1	−30 43 49	1.023	0.675	−0.016	−0.780	1

TABLE I. (continued)

Name	Lum	α (1950) δ		C4548	C4245	C4142	C3842	N_D
PHI4/2 68	III	12 48 04.4	−28 10 36	1.237	0.718	0.081	−0.552	1
PHI4/2 73	III	12 47 37.2	−28 29 32	1.136	0.656	0.028	−0.771	1
PHI4/2 89	V	12 46 12.5	−28 02 11	1.076	0.810	0.106	−0.456	1
PHI4/2 105	III/IV	12 45 21.0	−28 32 39	1.108	0.776	0.002	−0.648	3
PHI4/2 121	III	12 44 18.0	−29 12 19	1.271	1.023	0.153	−0.157	3
PHI4/3 1	III	12 40 40.7	−28 10 54	1.238	0.795	0.063	−0.508	2
PHI4/3 4	III	12 40 34.1	−28 39 59	1.165	0.799	0.046	−0.538	2
PHI4/3 13	III/IV	12 39 32.7	−28 14 45	1.128	0.770	0.046	−0.636	1
PHI4/3 15	III/IV	12 39 31.0	−28 13 30	1.175	0.872	0.035	−0.468	1
PHI4/3 18	V	12 39 18.6	−28 36 46	1.058	0.741	−0.021	−0.759	1
PHI4/3 20	III/IV	12 39 04.3	−28 04 55	1.112	0.784	−0.011	−0.679	1
PHI4/3 21	IV/V	12 39 08.1	−29 27 41	1.074	0.728	0.090	−0.561	1
PHI4/3 23	III/IV	12 38 54.7	−28 37 16	1.142	0.867	0.107	−0.404	1
PHI4/3 53	III/IV	12 37 05.0	−28 36 29	1.186	0.899	0.234	−0.277	1
PHI4/3 58	III	12 36 48.5	−29 20 45	1.242	0.959	0.139	−0.295	1
PHI4/3 86	V	12 34 23.1	−28 17 32	1.035	0.701	−0.005	−0.773	1
PHI4/3 89	IV/V	12 34 09.0	−28 08 39	1.049	0.683	0.019	−0.700	2

standards with a range in abundance and color were selected from the giant branches* of M67 ([Fe/H] = − 0.1) and ω Cen ([Fe/H] = − 1.6), with other observations made of NGC 3201 ([Fe/H] = − 1.6), NGC 6397 ([Fe/H] = − 1.8), and several bright solar abundance IAU standards as checks. In addition, a program star was selected as a local standard and observed on average twice per night. Arc spectra were taken before and after each exposure and used to rebin the spectra on to a log wavelength scale. Two templates with good S/N were prepared by shifting and adding all the rebinned M67 and ω Cen exposures. Radial velocities were obtained from the rebinned spectra using cross correlation techniques (with Fourier filtering) against these templates.

Most program stars were measured twice or more, from which we derive a standard error of 10 km s^{-1} for a single measurement. In addition, we obtained good agreement ($\approx$10 km s^{-1}) between our velocities for NGC 3201 and NGC 6397 and those in Webbink (1981), and Zinn and West (1984). To check the zero point of our velocities, J. Sommer-Larsen kindly obtained for us a coudé spectrum of our local standard at a resolution of 6 km s^{-1} channel^{-1} with the 1.9 m telescope. The random error on the coudé velocity was 2 km s^{-1}. Our mean Cassegrain velocities and the coudé velocity agreed to 3 km s^{-1}.

Heliocentric radial velocities (in km s^{-1}) for the giants and the number of measurements N_{rv} are shown in columns 5 and 6 of Table II; radial velocities for ten dwarfs are shown in Table III.

IV. DERIVED QUANTITIES

Abundance, distance and reddening estimates have been derived from the DDO and *BV* photometry. A detailed description of our methodology is given in Appendix A.

a) Abundance Measurement

DDO photometry gives a system for measuring abundance which has been calibrated against both the globular clusters, and field stars with fine analysis measures of [Fe/H], and which is applicable for [Fe/H] values from solar to − 2.3. We estimate our error on a single [Fe/H] value to be 0.25 dex (see Appendix A for justification of this estimate). Table II gives the [Fe/H] values (from DDO photometry) for all the giants in our survey.

An independent check of our DDO [Fe/H] values was provided by observations of eight stars from the 959 field, using the Anglo–Australian telescope with the IPCS/RGO spectrograph combination and a resolution of 2.5 Å. Values of the Ca II H and K index *A*(Ca) were calculated from the spectra, and [Fe/H] values derived using the calibration of Flynn and Morrison (1990). Table IV gives *A*(Ca) values and [Fe/H] values derived from *A*(Ca) for these stars: the mean difference between [Fe/H] from DDO and *A*(Ca) was 0.06, with a standard deviation (s.d.) of 0.33, which shows good agreement between the results of two independent methods.

b) Reddening

There were 17 stars in each field which were metal-strong enough to be suitable for use with the Janes (1977) reddening technique. In the PHI field the mean reddening was $E(B-V) = 0.021$, with a s.d. of 0.030 for the 17 stars: this would have made a negligible difference to the DDO colors and derived quantities, and so the reddening was assumed to be zero. However, in the 959 field, the mean reddening was $E(B-V) = 0.047$ (s.d. 0.041). Before we estimated [Fe/H], M_V and luminosity class for the 959 stars, the DDO colors were de-reddened using the color excess ratios of McClure (1979).

c) Distances and Luminosities

Appendix A describes the calculation of absolute magnitude for the giants. The *V* magnitudes (dereddened for the 959 field) were then used to calculate distance. Errors on distance were estimated by propagating our DDO and *BV*

*Abundances quoted here are from Taylor (1982) for M67 and Zinn and West (1984) for the other clusters.

TABLE II. The giants.

Name	V	$B-V$	N_{BV}	RV	N_{RV}	[Fe/H]	M_V	D
959 11 2	12.45	1.22	4	79	1	−0.88	0.32	2500
959 11 3	11.52	0.95	3	−58	1	−0.83	1.54	930
959 11 13	12.78	0.91	3	...	...	−0.81	2.03	1300
959 11 36	11.84	0.99	2	−5	2	−0.71	1.25	1200
959 11 39	10.82	1.02	2	−9	19	−0.66	1.33	740
959 11 51	11.47	0.98	2	−1	1	−0.95	1.38	980
959 11 58	11.92	0.88	5	−3	6	−0.84	2.32	790
959 11 81	11.54	1.05	2	−28	2	−0.40	2.70	550
959 11 94	11.24	0.85	2	−74	1	−1.29	1.46	850
959 11 142	12.11	0.91	3	−62	4	−0.79	2.11	940
959 11 163	12.31	1.37	4	−211	3	−1.06	−0.99	4300
959 12 44	12.68	0.79	1	−51	3	−1.54	1.55	1600
959 12 116	12.14	1.07	1	47	2	−0.39	1.57	1100
959 12 126	12.06	1.07	1	5	2	−0.46	1.68	1100
959 31 59	11.15	1.02	2	4	1	−0.24	2.18	580
959 31 77	11.78	1.05	2	−98	2	−0.49	1.40	1100
959 31 87	12.80	0.85	3	5	2	−1.22	1.60	1600
959 31 108	12.83	0.99	2	−11	2	−0.65	2.04	1300
959 31 167	11.08	1.00	2	−25	2	−1.76	−0.90	2300
959 31 176	12.66	0.97	1	37	2	−0.43	2.44	1000
959 31 190	12.41	1.43	1	−1	2	−0.69	0.27	2500
959 32 12	12.75	1.06	1	−42	2	−0.61	1.39	1800
959 32 22	12.76	1.02	2	−29	2	−0.45	1.21	1900
959 32 32	13.08	1.15	2	−58	2	−0.49	2.06	1500
959 32 43	12.83	1.37	2	−12	2	−0.28	1.52	1700
959 32 59	12.69	1.09	2	−72	2	−0.89	0.05	3200
959 32 69	12.51	1.08	2	−46	2	−0.45	2.62	890
959 32 78	11.76	1.00	6	−49	2	−0.42	2.78	590
959 32 87	11.38	1.33	7	−315	4	−1.20	−1.13	3000
959 32 98	12.17	0.87	3	−35	2	−1.26	1.45	1300
959 32 108	13.27	1.04	3	−13	2	−0.91	−0.17	4600
959 32 144	12.66	1.14	1	−68	2	−0.55	2.19	1200
959 32 154	13.18	1.01	2	−15	3	−0.57	2.09	1500
959 32 162	11.71	1.23	2	...	...	−0.02	1.32	1100
959 32 184	12.98	1.04	1	−72	2	−0.55	0.98	2400
959 32 190	13.18	1.01	2	−19	2	−0.66	1.65	1900
959 41 39	11.17	1.03	2	16	2	−0.52	1.65	750
959 41 128	12.09	1.10	2	−59	2	−0.46	1.19	1400
959 41 150	11.01	1.01	3	32	2	−0.58	1.35	800
959 41 175	10.83	1.09	2	−2	3	−0.51	1.23	780
959 42 2	12.46	0.92	1	−140	1	−1.53	0.07	2800
959 42 26	11.59	1.22	2	−17	3	−0.62	1.17	1100
959 42 49	11.16	1.00	2	−134	1	−0.79	1.70	730
959 42 72	12.42	1.02	1	−13	2	−1.72	−0.96	4500
959 42 78	12.44	1.01	2	38	3	−0.52	1.39	1500
959 42 99	11.69	1.24	2	−1	3	−0.65	0.62	1500
959 42 125	11.41	1.30	2	−1	2	−0.23	1.24	1000
959 42 134	12.01	1.07	4	−165	3	−1.32	−0.45	2900
959 42 186	11.12	1.06	2	−74	1	−0.59	2.28	550

TABLE II. (continued)

Name	V	$B-V$	N_{BV}	RV	N_{RV}	[Fe/H]	M_V	D
GPEC 106	11.08	0.79	2	160	1	−2.21	−0.29	1900
GPEC 465	11.01	0.89	1	−18	2	−0.48	3.12	380
GPEC 515	10.56	1.11	2	145	2	−1.83	−1.68	2800
GPEC 1172	11.58	0.72	2	149	2	−1.87	1.05	1300
GPEC 1206	11.99	0.91	2	104	2	−2.35	−1.25	4400
GPEC 1434	11.46	1.04	2	−26	2	−0.44	1.45	1000
GPEC 1834	11.78	0.85	2	74	2	−1.10	1.48	1100
GPEC 2045	10.79	0.96	2	247	3	−1.71	−0.86	2100
GPEC 2156	11.18	0.95	2	21	3	−0.53	0.99	1100
GPEC 2643	10.40	1.34	11	421	4	−2.09	−2.48	3800
GPEC 2650	11.02	0.87	16	59	6	−2.03	−0.67	2200
GPEC 2904	10.91	1.11	2	48	1	−1.93	−1.75	3400
GPEC 3038	11.31	0.91	2	290	2	−1.61	−0.38	2200
GPEC 3672	11.21	0.87	2	−57	3	−1.02	1.46	890
PHI2/1 43	12.61	0.98	3	245	1	−1.60	−0.87	5000
PHI2/1 49	12.59	1.07	1	−3	1	−0.68	1.17	1900
PHI2/1 52	13.06	0.87	2	227	1	−2.11	−0.74	5800
PHI2/1 66	13.32	0.83	3	−6	1	−1.35	1.00	2900
PHI2/1 69	13.21	1.02	2	46	1	−0.58	0.64	3200
PHI2/2 2	12.13	1.23	1	−1	1	−0.15	0.87	1800
PHI2/2 4	13.37	1.14	2	8	1	−0.83	0.26	4200
PHI2/2 7	13.37	1.02	2	105	1	−1.37	−0.57	6100
PHI2/2 8	13.43	1.08	2	−26	1	−0.69	1.14	2900
PHI2/2 10	11.62	1.13	1	−44	1	−0.50	1.36	1100
PHI2/2 19	12.11	1.00	2	−13	2	−0.52	1.13	1600
PHI2/2 23	12.75	1.19	2	322	2	−2.26	−2.31	10000
PHI2/2 31	12.91	1.14	2	16	2	−0.57	1.75	1700
PHI2/2 33	12.60	1.02	2	18	1	−0.55	1.15	1900
PHI2/2 40	12.75	1.00	3	28	1	−0.75	0.96	2300
PHI2/2 46	12.72	1.48	3	296	1	−1.34	−1.93	8500
PHI2/2 49	12.03	1.03	3	137	1	−1.09	−0.02	2600
PHI2/2 71	12.56	1.03	1	−5	1	−0.52	1.21	1900
PHI2/2 97	12.95	0.93	3	12	2	−1.10	0.67	2900
PHI2/2 100	12.59	0.96	3	...	...	−0.90	0.82	2300
PHI2/2 111	12.31	0.86	3	17	1	−0.09	2.76	820
PHI2/2 121	12.51	0.87	1	−32	1	−0.41	3.48	640
PHI4/1 7	11.91	1.36	2	25	1	−1.08	−1.11	4000
PHI4/1 19	12.47	0.96	2	−26	2	−0.58	1.80	1400
PHI4/1 21	12.80	0.83	1	202	1	−1.86	−0.10	3800
PHI4/1 62	13.08	0.99	3	27	2	−0.91	0.50	3300
PHI4/1 63	13.39	0.90	2	...	...	−1.17	0.76	3400
PHI4/1 65	13.27	0.77	1	93	1	−1.14	2.48	1400
PHI4/1 99	13.22	1.22	3	183	1	−2.01	−2.15	12000
PHI4/1 167	13.30	1.09	2	205	1	−1.71	−1.48	9100
PHI4/1 170	12.36	1.06	3	168	2	−1.41	−0.84	4300
PHI4/1 176	13.52	0.87	1	...	...	−1.16	1.13	3000
PHI4/1 178	12.72	0.95	3	231	1	−0.79	1.35	1900
PHI4/2 15	13.20	1.03	2	−19	1	−0.62	1.11	2600
PHI4/2 20	13.63	0.95	1	−33	2	−0.40	1.96	2200
PHI4/2 33	12.49	1.00	1	...	...	−0.30	3.27	700

TABLE II. (continued)

Name	V	$B-V$	N_{BV}	RV	N_{RV}	[Fe/H]	M_V	D
PHI4/2 34	13.56	0.93	2	−35	1	−0.93	1.40	2700
PHI4/2 35	13.48	0.87	3	...	...	−1.34	0.66	3700
PHI4/2 68	12.46	1.05	3	57	1	−2.01	−1.62	6600
PHI4/2 73	12.61	0.81	3	121	1	−1.82	0.14	3100
PHI4/2 105	13.61	0.86	1	−8	2	−0.61	2.85	1400
PHI4/2 121	12.18	1.27	3	86	1	−0.66	0.45	2200
PHI4/3 1	12.74	1.11	3	215	2	−1.67	−1.51	7100
PHI4/3 4	11.63	0.93	2	15	3	−0.95	0.98	1300
PHI4/3 13	13.00	0.89	2	53	2	−0.72	2.00	1900
PHI4/3 15	13.53	0.94	1	14	1	−0.74	1.70	2300
PHI4/3 20	13.34	0.86	2	−27	2	−0.68	2.80	1300
PHI4/3 23	11.76	0.98	1	−2	2	−0.27	2.80	620
PHI4/3 53	13.47	1.05	1	...	...	−0.02	1.44	2600
PHI4/3 58	13.42	1.15	2	72	1	−0.78	0.49	3900

Columns as follows: (1) star name; (2,3) photoelectric V and $B-V$ (no reddening correction applied); (4) N_{BV}, the number of BV observations; (5) RV, the heliocentric radial velocity in km s^{-1}; (6) N_{RV}, the number of radial velocity observations; (7,8,9) metallicity, absolute magnitude and distance (in parsecs).

photometric errors, and errors in [Fe/H] through the calculation of absolute magnitude. The average distance error was 23%, most were between 15% and 30%. Values of M_V and distance for each giant are given in Table II.

d) The Selection of Metal-Strong Giants Using the CN Bands

We note here an unavoidable selection effect for our metal-strong giants, with abundances in the range $0.0 < [\mathrm{Fe/H}] < -1.0$. As described in Flynn and Morrison (1990), these giants were found by looking for stars with $B-V > 1.0$ and with weakened CN bands. The bands are affected by metallicity, temperature, and intrinsic luminosity, in the sense that the more luminous and/or redder giants have stronger bands. Hence, our technique tended to locate bluer,
less luminous giants, as well as those poorer in metals. Our metal-strong giants are not as a consequence centered on the tangent point, but are approximately 2 kpc closer. A redder color cutoff would have compensated for this effect.

TABLE III. The dwarfs.

Name	RV[a]	N_{RV}[b]
959 12 121	4	1
959 31 119	0	1
PHI2/2 127	34	1
PHI2/2 132	4	1
PHI4/1 58	−5	1
PHI4/1 67	49	1
PHI4/1 106	8	2
PHI4/1 153	62	2
PHI4/1 177	−14	2
PHI4/3 86	−21	1

[a] Radial velocity in km s^{-1}.
[b] Number of observations.

V. ESTIMATION OF ROTATIONAL KINEMATICS

For consistency with the analysis of Frenk and White (1980), we adopt the standard spherical coordinate system (r, ϕ, θ), with r directed radially outward from the center of the Galaxy, ϕ in the direction of galactic rotation, and θ measured from the Galaxy's north pole. Since most of the sample is at relatively low z height and at a similar galactocentric distance as the Sun, the choice of coordinate system is not critical. We seek estimates of the mean rotational velocity V_{rot} and the velocity dispersion component σ_ϕ.

A pitfall of the standard techniques used to estimate these quantities is that they can be greatly affected by even small numbers of stars with extreme velocities. This is particularly relevant to the galactic halo, where recent work by Norris and Ryan (1989) has highlighted the existence of a small population of stars with extreme retrograde velocities. These stars will contribute far more than they should to the values of mean motion and velocity dispersion, unless special precautions are taken. Eddington (1914) was aware of this problem in estimation of velocity dispersion: "...squaring the

TABLE IV. A(Ca) (and [Fe/H] derived from A(Ca)) for stars in 959 field.

Name	A(Ca)	$[\mathrm{Fe/H}]_{A(\mathrm{Ca})}$	$[\mathrm{Fe/H}]_{\mathrm{DDO}}$
959 11 2	0.44	−1.27	−0.88
959 11 58	0.37	−1.14	−0.84
959 11 163	0.51	−0.69	−1.06
959 12 44	0.34	−1.16	−1.54
959 31 87	0.31	−1.66	−1.22
959 32 59	0.43	−0.98	−0.89
959 32 108	0.43	−0.81	−0.91
959 42 134	0.39	−1.50	−1.32

velocities exaggerates the effect of a few exceptional velocities." Recent statistical work on robust estimation provides simple techniques for dealing with outliers. We discuss the techniques in detail in Appendix B, and here note only that we use trimmed estimators, which order the data and remove the lowest and highest 5%, before calculating the kinematical quantities of interest. (Compensation is made for the trimming where necessary in order to produce unbiased estimates.) We thus sacrifice a small amount of our data, but safeguard against producing results that are severely biased by a few unusual stars.

a) Geometry

For completeness, we include the formulas that describe the three-dimensional geometry of the situation. Derivations can be found in Frenk and White (1980) and Woolley (1978). Assume that the star has galactic longitude and latitude (l,b) and is at a distance of R kpc from the Sun. We convert its line-of-sight velocity to $V_{\rm gal}$, the velocity as seen by an observer at rest with respect to the galactic center, by correcting for the Sun's motion with respect to the local standard of rest (LSR), and the circular velocity of the LSR around the galactic center. $V_{\rm LSR}$ is assumed to be 220 km s^{-1}; we assume that the Sun moves with a velocity of 15.4 km s^{-1} towards $l = 51°$, $b = 23°$ (Delhaye 1965), and let $V_{\rm corr}$ be the velocity corrected for the solar motion.

Then $V_{\rm gal}$ can be written:

$$V_{\rm gal} = V_{\rm corr} + V_{\rm LSR} \cos b \sin l. \tag{1}$$

Expressing this velocity in spherical polar coordinates:

$$V_{\rm gal} = \alpha V_r + \beta V_\phi + \gamma V_\theta. \tag{2}$$

To obtain explicit expressions for α, β, and γ, we assume the distance from the Sun to the galactic center ($R_\odot$) is 8.5 kpc, and use the quantities r (the distance from the star to the galactic center), and u (the projection of this distance on the galactic plane):

$$r^2 = R_\odot^2 + R^2 - 2RR_\odot \cos b \cos l, \tag{3}$$

$$u^2 = R_\odot^2 + R^2 \cos^2 b - 2RR_\odot \cos b \cos l, \tag{4}$$

$$\alpha = (1/r)(R - R_\odot \cos b \cos l), \tag{5}$$

$$\beta = (1/u)(R_\odot \cos b \sin l), \tag{6}$$

$$\gamma = (\sin b / ur)(RR_\odot \cos b \cos l - R_\odot^2). \tag{7}$$

b) Estimation of $V_{\rm rot}$

We extend Frenk and White's (1980) estimation of $V_{\rm rot}$ by trimming outliers, and then calculating $V_{\rm rot}$ using their method. The quantity $\beta V_{\rm gal}$ is calculated for each star. Note that multiplying by β gives highest weight to the stars whose line-of-sight velocity contains mostly V_ϕ. Frenk and White comment that in the simplest case where the residual velocity distribution (after removal of terms involving systemic rotation and expansion) is independent of position in the Galaxy, this is a minimum variance estimate; we also checked this empirically using Monte Carlo simulations with various choices of weighting factor. Estimates using β had the lowest error. The $\beta_i V_{{\rm gal},i}$ are then ordered, and the lowest and highest 5% are removed. The estimate of $V_{\rm rot}$ ($\hat{V}_{\rm rot}$) is calculated using the following formula (with the subscript i ranging over all values which have not been trimmed):

$$\hat{V}_{\rm rot} = \frac{\Sigma_i \beta_i V_{{\rm gal},i}}{\Sigma_i \beta_i^2}. \tag{8}$$

c) Estimation of σ_ϕ

The estimation of $V_{\rm rot}$ is made simpler by the fact that we assume the mean r and θ motions in the Galaxy to be zero (no net expansion or contraction, or mean z motion). This means that $V_{\rm gal}/\beta$ will give an unbiased estimate of V_ϕ for a single star. However, since the mean values $\langle V_r^2 \rangle$ and $\langle V_\theta^2 \rangle$ are nonzero, the velocity dispersion of the observed velocities will not give an unbiased estimate of σ_ϕ but will be larger due to contributions from σ_r and σ_θ. We need to correct for this bias. We have assumed values for σ_r and σ_θ which have been constrained by other kinematical research and we will examine the effect of changing these values in the next section.

The velocity ellipsoid has been assumed to be constant and aligned along the spherical coordinate system at all points in the Galaxy.

Since the stars in our sample are not all optimally placed at the tangent points, we follow Frenk and White's procedure of weighting the data values by the projection factor associated with V_ϕ [β in Eq. (2)] in our calculation of velocity dispersion. Once again, empirical checks using Monte Carlo simulations confirmed that this choice of weighting factor produced the best estimates.

To estimate σ_ϕ, we calculate the same quantity $\beta_i V_{{\rm gal},i}$ for each star, order and remove the lowest and highest 5%, and then calculate the velocity dispersion of these weighted quantities:

$$\sigma_{{\rm gal},w}^2 = \frac{1}{n_{\rm trim} - 1} \sum_i \left(\beta_i V_{{\rm gal},i} - \frac{\Sigma \beta_i V_{{\rm gal},i}}{n_{\rm trim}} \right)^2, \tag{9}$$

where the subscript i ranges over all observations which have not been trimmed, and $n_{\rm trim}$ is the number of observations after trimming.

It can be shown that, if n is the total number of observations before trimming, the expected value of $\sigma_{{\rm gal},w}^2$ is

$$E(\sigma_{{\rm gal},w}^2) = \sigma_r^2 \frac{\Sigma \alpha_i^2 \beta_i^2}{n} + \sigma_\phi^2 \frac{\Sigma \beta_i^4}{n} + \sigma_\theta^2 \frac{\Sigma \beta_i^2 \gamma_i^2}{n} + \frac{V_{\rm rot}^2}{(n-1)} \left(\Sigma \beta_i^4 - \frac{(\Sigma \beta_i^2)^2}{n} \right), \tag{10}$$

where the index i now ranges over the whole sample, not just the trimmed sample, and n is the total number of observations before trimming. If $\hat{V}_{\rm rot}$ is the estimate obtained previously, and values of σ_r and σ_θ are assumed, then ($\hat{\sigma}_\phi$), is given by

$$\hat{\sigma}_\phi^2 = \frac{n}{\Sigma \beta_i^4} \left[\sigma_{{\rm gal},w}^2 - \sigma_r^2 \frac{\Sigma \sigma_i^2 \beta_i^2}{n} - \sigma_\theta^2 \frac{\Sigma \beta_i^2 \gamma_i^2}{n} - \frac{(\hat{V}_{\rm rot})^2}{(n-1)} \left(\Sigma \beta_i^4 - \frac{(\Sigma \beta_i^2)^2}{n} \right) \right]. \tag{11}$$

We have checked that this procedure does in fact produce unbiased estimates of σ_ϕ using Monte Carlo simulations. These simulations assigned a random velocity to "stars" at the position and distance of each star in the sample, thus simulating the real data closely. The chosen weighting scheme ensures that efficient use is made of the available observations.

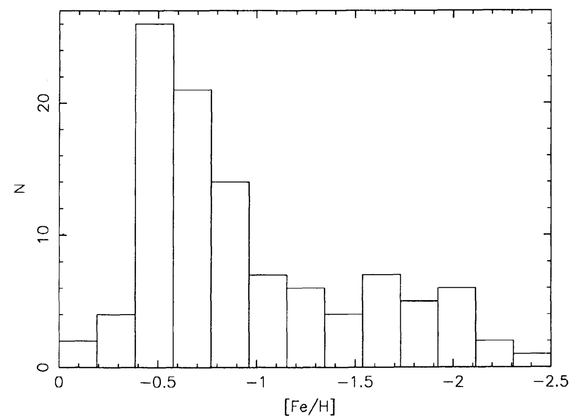

FIG. 1. The abundance distribution for our sample of giants. Note that the sample is not representative of the true abundance distribution, since our technique was biased toward the discovery of metal-weak objects.

d) Estimation of Errors

We also used Monte Carlo simulations to produce error estimates for $V_{\rm rot}$ and σ_ϕ, as it is difficult to work out errors analytically in the case of σ_ϕ. The procedure is as follows: the estimates $\hat{V}_{\rm rot}$ and $\hat{\sigma}_\phi$ are calculated. A sample is simulated by taking the positions on the sky (l,b) of the stars in the sample, and randomly assigning values of V_r, V_θ, and V_ϕ to each "star" from Gaussian distributions with

$$\langle V_r \rangle = \langle V_\theta \rangle = 0,$$

$$\langle V_\phi \rangle = \hat{V}_{\rm rot},$$

σ_r, σ_θ as assumed in the calculation of $\hat{\sigma}_\phi$,

$$\sigma_\phi = \hat{\sigma}_\phi.$$

The star's original distance has a random number added to it to simulate a 23% distance error. Values of α, β, and γ are calculated, using the randomized distance, and then $V_{\rm gal}$ is calculated. $V_{\rm gal}$ has a random number added to it to simulate a measuring error of 10 km s^{-1} on the radial velocity.

This simulated sample is used to work out estimates of $V_{\rm rot}$ and σ_ϕ. The process is repeated 200 times, and the s.d.'s of the simulated $V_{\rm rot}$ and σ_ϕ distributions give error estimates for $\hat{V}_{\rm rot}$ and $\hat{\sigma}_\phi$. We find that our estimates of error for $\hat{V}_{\rm rot}$ are within 1-2 km s^{-1} of the error estimates obtained using the Frenk and White formalism.

e) A Check Using Nearby Dwarfs

We have calculated $V_{\rm rot}$ and σ_ϕ for the dwarfs in the sample with radial velocities (Table III). [Their distances were calculated from photographic magnitudes and by transforming DDO C4245 colors to $B-V$ and then determining their absolute magnitudes M_V from the disk main sequence of Bahcall (1986).] For 10 dwarfs with mean distance of 400 pc ($z = 200$ pc), $V_{\rm rot} = 216 \pm 13$ km s^{-1}. Assuming $\sigma_r = 40$ km s^{-1} and $\sigma_\theta = 20$ km s^{-1} gives $\sigma_\phi = 29 \pm 13$ km s^{-1}. These values are consistent with previous determinations for disk dwarfs [see, e.g., Fuchs and Wielen (1987)].

VI. THE KINEMATICS OF OUR SAMPLE

The [Fe/H] distribution for the giants from our sample is shown in Fig. 1. Two components can be seen: one with a small spread in [Fe/H] which peaks at [Fe/H] $= -0.5$, and one with a large spread in [Fe/H], centered on [Fe/H] $\simeq -1.7$. If abundance were a sufficient criterion to classify stars as belonging to the disk, thick disk, or halo, we might expect the peak at [Fe/H] $= -1.7$ to correspond to the halo, and the peak at [Fe/H] $= -0.5$ to the thick disk. In what follows, we will divide the stars into different abundance groups, and investigate the kinematics of each group, to see whether the division is reasonable.

There are 67 giants with [Fe/H] > -1.0, and 38 with [Fe/H] < -1.0. The mean galactocentric distance of the giants in our sample is 8 kpc, and their heights above the plane range from 200 pc to 6.3 kpc. The dependence of z height on [Fe/H] can be seen in Fig. 2, where the filled circles denote stars from our sample. The intrinsically fainter metal-strong giants are concentrated at low z height, as we would expect in this magnitude-limited sample.

It can be seen from Fig. 1 that there are only a small number of stars more metal strong than [Fe/H] $= -0.5$. This is caused by our method of selection of giants; since the procedure was optimized for discovery of halo giants, the probability of selection is greatest for the metal-weakest stars and decreases as [Fe/H] increases. Estimates of completeness of the halo sample will be given in Morrison (1990); we note here that the sample is not complete at the metal-strong end.

Radial velocities $V_{\rm corr}$ (corrected for the solar motion with respect to the LSR) have been plotted versus abundance in Fig. 3. We have reversed the signs of the radial velocities from the PHI field (aligned toward galactic antirotation) so that they may be plotted with the velocities from the 959 field (aligned toward galactic rotation). Note the following features in this diagram: at high abundances, from solar to [Fe/H] $\simeq -0.7$, the stars are on rapidly rotating orbits and have a low line-of-sight velocity dispersion. For convenience, we refer to these two properties as "disk kinematics" in what follows. The metal-weak stars (less than [Fe/H] $\simeq -1.4$) have close to zero rotation, and a high line-of-sight velocity dispersion. This we designate "halo kinematics." However, in the intermediate region ($-0.7 \geqslant$ [Fe/H] $\geqslant -1.4$), there are relatively more stars with high rotation ($V_{\rm corr} \simeq 0$) than in the region with [Fe/H] < -1.4. We are looking at a region of overlap in abundance between the halo and the disk.

How far does this region stretch toward low abundance? We examine this question by using the velocity histograms of Fig. 4. Such histograms provide a useful exploratory tool, as they contain much more information than the two summary statistics usually quoted ($V_{\rm rot}$ and σ_ϕ). They show both the shape of the velocity distribution and the importance (or otherwise) of stars with extreme velocities.

We postulate a simple description for the disk and halo, with roughly symmetric velocity distributions for the pure disk and halo. If the abundance distribution of the rapidly rotating objects overlaps that of the slowly rotating ones, the resulting velocity distribution in the overlap region will be skewed. We therefore use the asymmetry of the velocity distribution as a diagnostic—if a distribution is strongly asymmetric, it is possible that it is a mixture of disk and halo. (We treat asymmetry more thoroughly using statistical techniques in the next section.)

Figure 4 shows histograms of an unbiased estimate of V_ϕ, defined as:

$$\hat{V}_\phi = V_{{\rm gal},i}/\beta_i, \qquad (12)$$

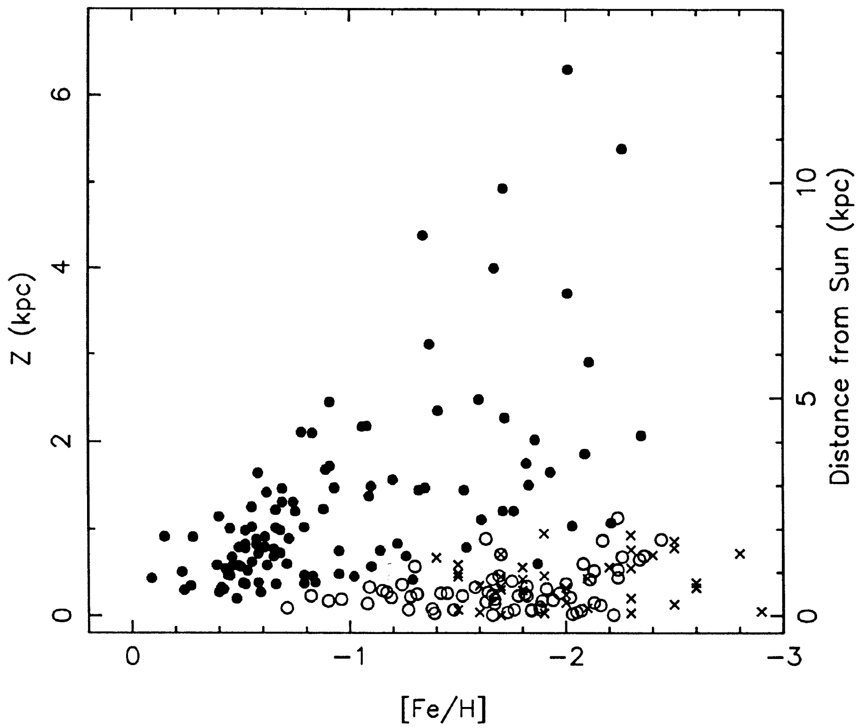

FIG. 2. The distance from the galactic plane $|z|$ plotted vs abundance, for our giants (filled circles) and for the giants of NBP (open circles) and Carney and Latham (1986) (crosses). Distance from the Sun is also shown for our giants.

for different abundance bins [see Eqs. (2) and (6)]. The values of velocity are not weighted (as in Sec. V). Instead, we have removed ten stars which are a long way from the tangent point, using the criteria $[Fe/H] < -0.8$, and $(|\alpha| + |\gamma|)/|\beta|) > 1.1$; this cutoff corresponds to an error of $\simeq 85$ km s^{-1} for V_ϕ. Only stars with $[Fe/H] < -0.8$ were removed, because the potential error due to the other components of the velocity ellipsoid is some 2–3 times larger for the high-velocity metal-weak stars compared to the metal-strong ones.

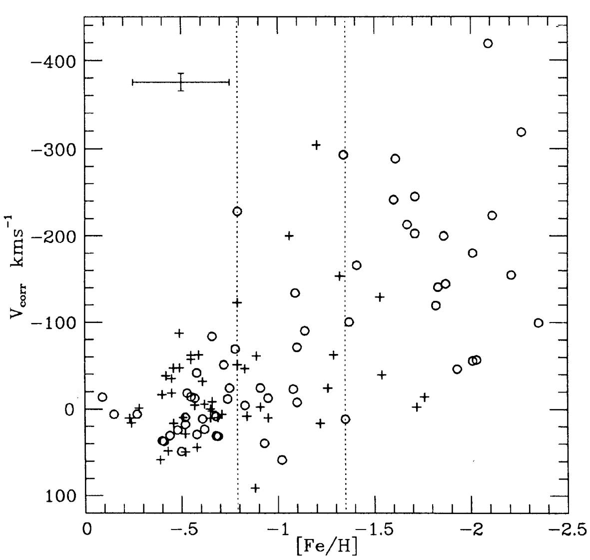

FIG. 3. Radial velocities V_{corr} corrected for the solar motion relative to the local standard of rest plotted vs abundance for our sample of giants. The sign of V_{corr} has been reversed for the stars in the antirotation field. The dashed lines indicate the abundance range which appears to contain stars of two kinematic types shown in Fig. 4(c). Crosses are stars from the 959 field, circles stars from the PHI field or Gpec stars.

We chose the abundance bins for the velocity histograms in Fig. 4 as follows: the highest abundance for a star with "high velocity" is at $[Fe/H] = -0.79$, so we divided the stars with abundances between 0.0 and -0.78 into two bins of equal size. Figure 4(a) shows stars with $0.0 > [Fe/H] > -0.55$. The velocities are characteristic of the old disk; they are symmetrically centered on $V_{rot} = 214 \pm 10$ km s^{-1}, with a low spread in velocity and a mean z height of 580 pc. Figure 4(b) shows the metal-weaker group with $-0.55 \geqslant [Fe/H] > -0.79$. The mean velocity has shifted to 185 ± 10 km s^{-1} and the spread has not changed significantly. The mean z height of these stars is 960 pc.

We examined the histogram of velocities for $[Fe/H] \leqslant -0.79$, and found that it was strongly skewed. It was only when we reduced the upper metallicity cutoff by using stars with $[Fe/H] \leqslant -1.35$ that the velocity distribution became more symmetric; this distribution is shown in Fig. 4(d). Thus we tentatively associate the stars with $[Fe/H] \leqslant -1.35$ with the halo, and use them to estimate halo kinematics for this sample. The intervening region $(-0.79 \geqslant [Fe/H] \geqslant -1.35)$ is shown in Fig. 4(c)—its strong asymmetry and modal value of $V_\phi \approx 200$ km s^{-1} [the same as that for the metal-stronger stars in Fig. 4(b)] suggests that we are seeing here a mixture of two discrete populations with disk and halo kinematics. A similar impression is given by the distribution of stars in Fig. 3. Although this is not the only possible way to interpret our data, we will present more evidence to support our description in the next section.

Another possible explanation for the distribution in Fig.

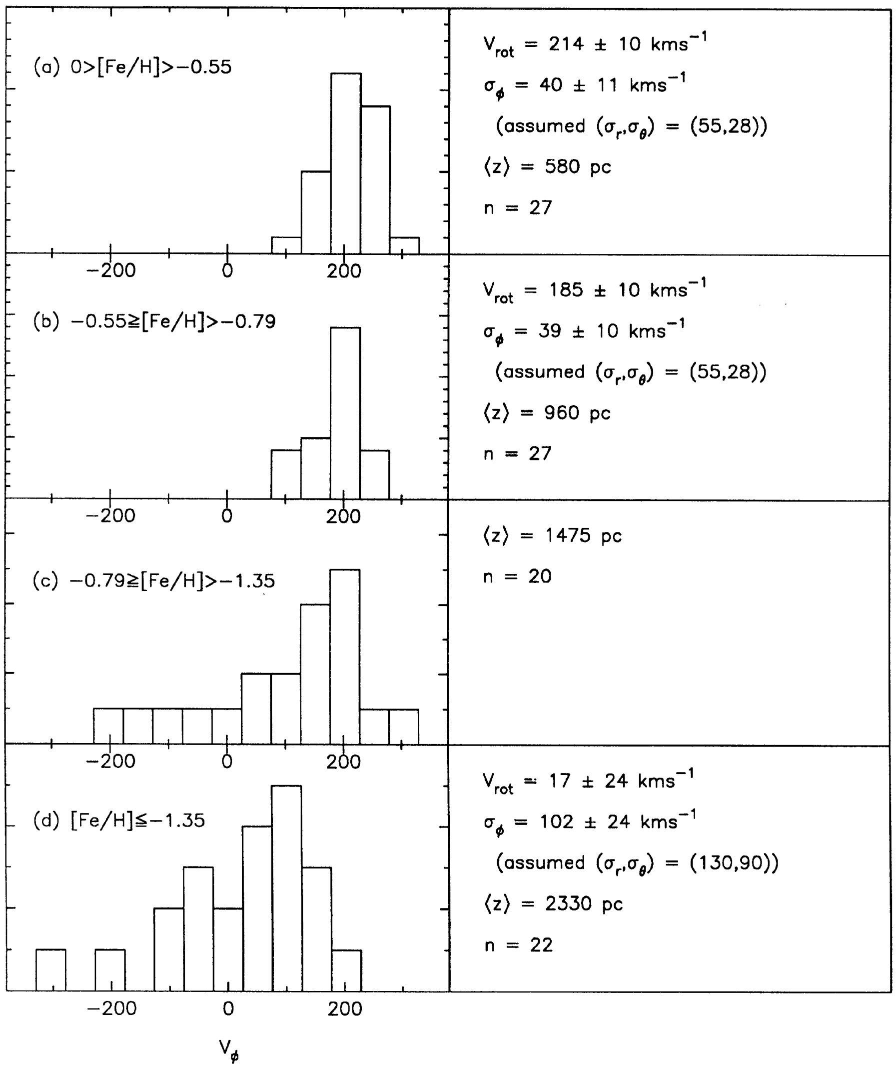

FIG. 4. Velocity histograms for four ranges in abundance for our giants. $\hat{V}_\phi$ is an unbiased estimator of Galactocentric rotation. One tick mark on the Y axis corresponds to one star. (a) and (b) both show disk kinematics, while (d) shows halo kinematics. Since these three histograms show symmetric distributions, our measurements of V_{rot} and σ_ϕ are shown in the right-hand panels. (The assumed values for the other two components of the velocity ellipsoid and mean z height are also shown.) (c) appears to be a mixture of stars from the two kinematic types, so no estimate of V_{rot} or σ_ϕ has been made.

4(c) is that abundance errors have moved metal stronger stars into this bin. We can estimate the effect of abundance errors from stars of true [Fe/H] $= -0.5$, where most of our disk stars lie. There are nine stars in Fig. 4(c) with $\hat{V}_\phi \geqslant 150$ km s^{-1}. These stars are uniformly spread in abundance from -0.79 to -1.34, so we assume an average abundance of [Fe/H] $= -1.0$. If a star has a true abundance of -0.5, and a measured abundance of -1.0, then the abundance error is 0.5 dex—twice our estimated error for [Fe/H]. If the error distribution is Gaussian, then for all nine stars to be seen at these abundances merely due to errors in [Fe/H] we need 390 stars at [Fe/H] $= -0.5$. In fact, there are 26 stars at this abundance. Therefore, we cannot explain these stars merely by abundance errors, unless the disk stretches much lower in abundance than [Fe/H] $= -0.5$.

Estimates of V_{rot} and σ_ϕ are shown on the right of Fig. 4 for each abundance range. (Note that the ten stars not shown in the velocity histogram have been included in the estimation, but with low weight.) The estimates are not shown for Fig. 4(c), because they do not give a satisfactory representation of a distribution which we believe contains two components. The velocity dispersion estimates have been corrected for the random measuring error in the velocities (10 km s^{-1}).

In order to calculate σ_ϕ, values of σ_r and σ_θ need to be assumed. For the halo, we assumed $(\sigma_r, \sigma_\theta) = (130, 90)$. These values are similar to those derived for stars with [Fe/H] < -1.2 in the solar neighborhood by Norris (1986). We derive $\sigma_\phi = 102 \pm 24$ for [Fe/H] $\leqslant -1.35$ [Fig. 4(d)]. These results are insensitive to the assumed $(\sigma_r, \sigma_\theta)$: to demonstrate this, we then computed estimates of σ_ϕ assuming that $(\sigma_r, \sigma_\theta) = (150, 110)$ and $(110, 60)$. σ_ϕ was 11 km s^{-1} lower for the first case, and 12 km s^{-1} higher for the second case: compared to an error of 24 km s^{-1} on σ_ϕ for this abundance interval, this is not significant.

The metal-stronger stars are not located optimally for measuring σ_ϕ, and we need to make stronger assumptions to constrain our answers. There is good evidence to suggest that the components of the velocity ellipsoid for the local disk $(\sigma_r, \sigma_\phi, \sigma_\theta)$ rise slightly with decreasing abundance,

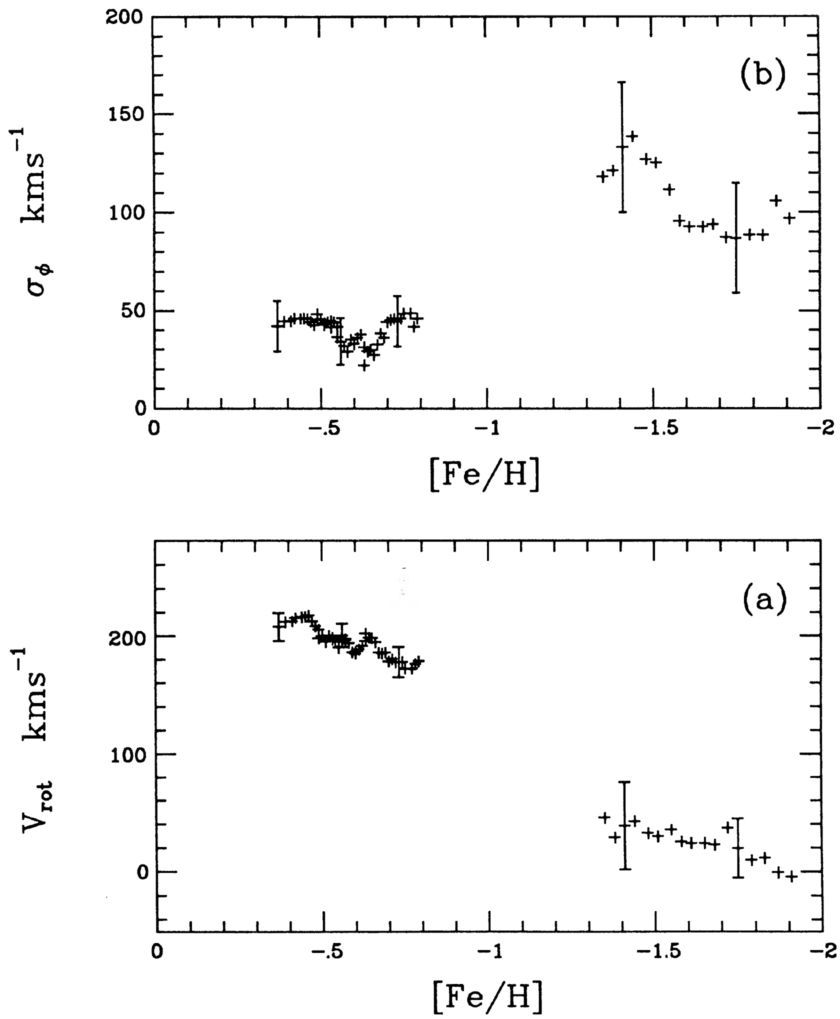

FIG. 5. (a) V_{rot} and (b) σ_ϕ plotted as functions of abundance. No calculation of σ_ϕ has been made in region where the velocity distribution appears asymmetric.

while the ratio of the three components remains close to 2:√2:1 (see, e.g., Janes 1975; Fuchs and Wielen 1987; Strömgren 1987). Since the stars in Figs. 4(a) and 4(b) are on rapidly rotating orbits, these assumptions are likely to hold.

We have solved for σ_ϕ from the line of sight velocity dispersion in an iterative manner, assuming values of $(\sigma_r, \sigma_\theta)$ which are in the ratio 2:1, solving for σ_ϕ from the line-of-sight velocity dispersion, and iterating until the assumed $(\sigma_r, \sigma_\theta)$ and the derived σ_ϕ were in the ratio 2:√2:1, within the errors given by the estimation of σ_ϕ. These results were more sensitive to the assumed values than those for the metal weaker stars; varying σ_r by ± 20 km s^{-1} has the effect of varying σ_ϕ Eq. (11) by ∓ 10 km s^{-1}.

Our estimates of σ_ϕ for both "disk" histograms are shown in Figs. 4(a) and 4(b). For both abundance ranges the same value of σ_ϕ was found. We quote $\sigma_\phi = 40 \pm 10$ km s^{-1} in the range $0.0 > [\mathrm{Fe/H}] > -0.78$.

In summary, we have found that the stars in the abundance range $-0.55 \geqslant [\mathrm{Fe/H}] > -0.78$, which have a mean height above the plane of ~ 1 kpc, have an asymmetric drift of 35 ± 10 km s^{-1}, and an azimuthal velocity dispersion of 40 ± 10 km s^{-1}. These kinematical quantities are consistent with membership of the thick disk, and in particular agree with the asymmetric drift derived by Ratnatunga and Freeman (1989).

Figure 5 shows the run of V_{rot} and σ_ϕ with abundance in more detail. The stars were ordered by abundance, and V_{rot} and σ_ϕ calculated by stepping down one star at a time with a "window" of 20 stars. Each point in the graph thus comes from a group of 20 stars centered on the plotted [Fe/H] value. This procedure smooths our data, and is a convenient way of showing the effect of binning.

In Fig. 5(a) we see a slow decrease of V_{rot} with decreasing abundance, from 214 ± 10 km s^{-1} at $[\mathrm{Fe/H}] \approx -0.4$ to 185 ± 10 km s^{-1} at $[\mathrm{Fe/H}] \approx -0.7$. This decrease is only marginally significant. We have not plotted estimates in the overlap region $-0.79 > [\mathrm{Fe/H}] > -1.35$ because the evidence points to an overlap of disk and halo here, so a single V_{rot} has little physical meaning. This impression is very strongly supported by the maximum-likelihood analysis described in Sec. VII. For $[\mathrm{Fe/H}] < -1.35$, V_{rot} is constant at approximately 15 ± 25 km s^{-1}.

Estimates of σ_ϕ (using the same assumptions as above) are shown in Fig. 5(b). Again, we have not plotted estimates in the overlap region. It can be seen that the estimates of σ_ϕ shown in Fig. 4 are not affected by choice of abundance bin.

We concluded above that the stars in the abundance range $-0.55 \geqslant [\mathrm{Fe/H}] > -0.78$ have properties consistent with membership of the thick disk. It is possible to estimate the radial scale length of this population using our measured asymmetric drift, and the components of its velocity ellipsoid. Friel (1989) has suggested that the thick disk may have a smaller radial scale length than the old disk (however, see also Ratnutunga and Freeman 1989). For a rotating population whose asymmetric drift is small relative to the velocity of the LSR, the following formula applies (Oort 1965):

$$V_{\rm LSR} - V_{\rm rot} = -\frac{\sigma_r^2}{2V_{\rm LSR}}\left(1 - \frac{\sigma_\phi^2}{\sigma_r^2} - \frac{2R}{h_R}\right). \qquad (13)$$

The asymmetric drift is given by $V_{\rm lag} = V_{\rm LSR} - V_{\rm rot}$, the scale length of the disk is h_R, and R kpc is the distance of the object from the galactic center.

To solve for h_R, we need the asymmetric drift $V_{\rm lag}$ (derived from our data to be 35 ± 10 km s^{-1}), the average distance of the stars from the galactic center (8 kpc in this sample), and the radial and azimuthal velocity dispersions σ_r and σ_ϕ. We derived a value of $\sigma_\phi = 40 \pm 10$ km s^{-1} from our data, using the constraint that $\sigma_r{:}\sigma_\phi = 2{:}\sqrt{2}$, and an assumed value of $\sigma_r = 55$ km s^{-1}. While we have assumed $\sigma_r = 55$ km s^{-1}, its value cannot be varied by more than ± 10 km s^{-1}, without violating the constraint $\sigma_r{:}\sigma_\phi = 2{:}\sqrt{2}$ (within the error on σ_ϕ). This is important because the derived value of h_R is quite sensitive to σ_r, and the ± 10 km s^{-1} will be used, along with the errors on $V_{\rm lag}$ and σ_ϕ to estimate the error on h_R.

Substituting the above values into Eq. (13) gives a radial scale length for these stars of 3 ± 1 kpc. This should be compared with estimates of h_R for the old disk of 5.0 ± 1.0 kpc (van der Kruit 1988) and 4.4 ± 0.3 kpc (Lewis and Freeman 1989). This gives some indication that the radial scale length of these stars, which we have associated with the thick disk, is smaller than that of the old disk [we note, however, that Ratnutunga and Freeman (1989) derived a lower limit of ≈ 4.5 kpc for the scale length of the thick disk, based on slightly different assumptions]. We shall see in Sec. VII*b5* that the impression of a smaller scale length is confirmed when we analyze a larger sample of stars.

In summary, our sample shows the following properties for disk stars:

(a) $V_{\rm rot}$ decreases slightly, from 214 ± 10 to 185 ± 10 km s^{-1} as [Fe/H] decreases from -0.3 to -0.7.

(b) If $(\sigma_r, \sigma_\theta) = (55, 28)$, then σ_ϕ is constant at 40 ± 10 km s^{-1} for this abundance range. The error in this result is the statistical uncertainty only. The result is additionally uncertain to the extent that a change of ± 20 in σ_r results in a change of ∓ 10 in σ_ϕ.

(c) Stars at the metal-weaker end of this abundance range ($-0.55 \geqslant$ [Fe/H] > -0.79) have kinematical properties consistent with membership of the "thick disk": an asymmetric drift of 35 ± 10 km s^{-1} and $\sigma_\phi = 40 \pm 10$ km s^{-1}.

(d) The radial scale length of the thick disk, derived from their kinematics, is 3 ± 1 kpc, a value which is slightly smaller than those derived recently for the thin disk.

For the halo, which we define for this sample as stars with [Fe/H] $\leqslant -1.35$, the main properties are:

(a) $V_{\rm rot} = 17 \pm 24$ km s^{-1}, and

(b) $\sigma_\phi = 102 \pm 24$ km s^{-1},

given that $(\sigma_r, \sigma_\theta) = (130, 90)$. (The result is not highly sensitive to this assumption.)

The shape of the histogram in the overlap region, ($-0.79 >$ [Fe/H] > -1.35), can be understood as an overlap of the pure disk and halo summarized above, and is not an artifact of abundance errors. We shall discuss this region further in the next section, using a considerably larger sample of stars. We will see that the relative numbers of disk and halo stars depend on *z* height, as we would expect. Close to the plane, the disk component is visible to [Fe/H] values as low as -1.6. This larger sample will lead us to redefine the abundance regions appropriate to each component at different heights above the plane.

VII. AN ENLARGED SAMPLE OF METAL-WEAK STARS

In the overlap region between the disk and the halo, we might expect to see a change in kinematical properties with *z* height, since the disk density falls off with *z* much faster than the halo. Our sample by itself is not suited for studying this effect, because we have few stars with [Fe/H] < -1.0 and $|z| < 1$ kpc. However, since our giants have a mean galactocentric distance of 8 kpc, it is reasonable to combine them with solar neighborhood samples of metal-weak stars. All the additional stars we have chosen were discovered by means of objective prism surveys (and so are free of kinematical selection effects) and all have abundance measurements of the same standard of accuracy as our DDO abundances.

We will use this enlarged sample to show that there is a strong dependence of kinematics on *z* height for *metal-weak* stars ([Fe/H] < -1.0).

a) The Enlarged Sample

We have added to our sample:

(a) The giants of NBP—for consistency, we applied exactly the same procedure for estimation of [Fe/H] and distance to these giants as we applied to our stars. The main difference from the published NBP results is that the new [Fe/H] values are on average 0.2 dex higher. (See Appendix A for discussion of this point.) We selected all giants with published *U*, *V*, and *W* values, and supplemented the sample by selecting (from those without space velocities) nine stars whose radial velocity is dominated by the V_ϕ component (using the same criterion as for our giants, described below). [Fe/H] values for the NBP giants we used range from -0.7 to -2.4, and their mean [Fe/H] is -1.7.

(b) The metal-weak red giants for which Carney and Latham (1986) have published space velocities. We selected all giants with abundances published by Bond (1980) and distances of less than 1 kpc from the Sun. (This keeps velocity errors low without introducing kinematic selection effects.) We show in Appendix A (see Fig. 14) that our DDO abundances are on the same scale as Bond's. The Carney and Latham sample has lower abundances: [Fe/H] values range from -1.4 to -2.9, and the mean value is -2.0.

We considered adding the NBP dwarfs to the extended sample, but decided that since there is no direct method of checking that dwarf and giant abundances are on the same scale, it would be safer not to use them. Hence the enlarged sample is composed entirely of G and K giants.

To make errors on V_ϕ from our original sample roughly comparable to errors from the other data, we omitted the ten stars from our sample which are far from the tangent point, using the same criteria as we did for presentation of Fig. 4 (roughly, an error in V_ϕ of less than 85 km s^{-1}).

For the stars with *U*, *V*, and *W* velocities, we estimated V_ϕ by $V + 231$ km s^{-1} (derived from our adopted solar motion and $V_{\rm LSR}$). For stars with radial velocities only, we used the estimate $\hat{V}_\phi$ defined in Eq. (12).

It is not immediately clear that estimates of V_ϕ from the velocity component V and from the radial velocity can be combined to make one sample. However, the errors on both estimates are not systematic, and they have the same size on average. For the velocity component $\hat{V}$, we used the published errors: for $\hat{V}_\phi$ we took into account the contamination from V_r and V_θ, and the measuring error on radial velocity. V_r and V_θ contribute only via their velocity dispersion, since mean motions in these directions are assumed zero. For stars with $[Fe/H] < -0.8$, we assume $(\sigma_r, \sigma_\theta) = (130, 90)$, and for stars with $[Fe/H] \geqslant -0.8$ we assume $(\sigma_r, \sigma_\theta) = (55, 28)$.

b) The Dependence of Kinematics on z Height

Figure 2 shows how well the solar neighborhood stars complement ours; for $[Fe/H] < -1.0$ the entire $|z|$ range from 0 to $\geqslant 2$ kpc is now represented. We now have a sample containing 199 stars.

We divided this sample into groups with $|z|$ above and below 1 kpc, and plot [Fe/H] against V_ϕ for each group in Fig. 6. There is a remarkable difference between the kinematics of the stars in the two diagrams. For $|z| \geqslant 1$ kpc, there is an abrupt change at $[Fe/H] \simeq -1.0$ between disk and halo kinematics; little or no overlap between the populations is visible. The stars with $|z| < 1$ kpc have very different motions; there is a significant overlap between disk and halo kinematics, starting at $[Fe/H] \simeq -0.8$ and stretching as low as $[Fe/H] = -1.6$. This region contains the metal-weak stars in near-circular orbits remarked upon by NBP (with planar eccentricity $e < 0.4$ and $[Fe/H] < -1.2$). There are additional stars with disk kinematics in this region from both our sample and that of Carney and Latham, confirming the NBP result. Below $[Fe/H] = -1.6$, the stars have close to zero net rotation but, curiously, do not appear to be well mixed in the V_{rot}–[Fe/H] plane. Larger samples would be needed to confirm the reality of this impression.

We obtain further insight into the kinematics of the two samples by examining the velocity histograms of Fig. 7. The four panels on the left show different abundance ranges for stars with $|z| < 1$ kpc; the three on the right show the same abundance ranges for stars with $|z| \geqslant 1$ kpc. There are no stars in the latter sample in the highest abundance bin, because of the magnitude limit of our sample.

If a velocity distribution is symmetric, we estimated the mean rotational velocity using a 5% trimmed mean (see

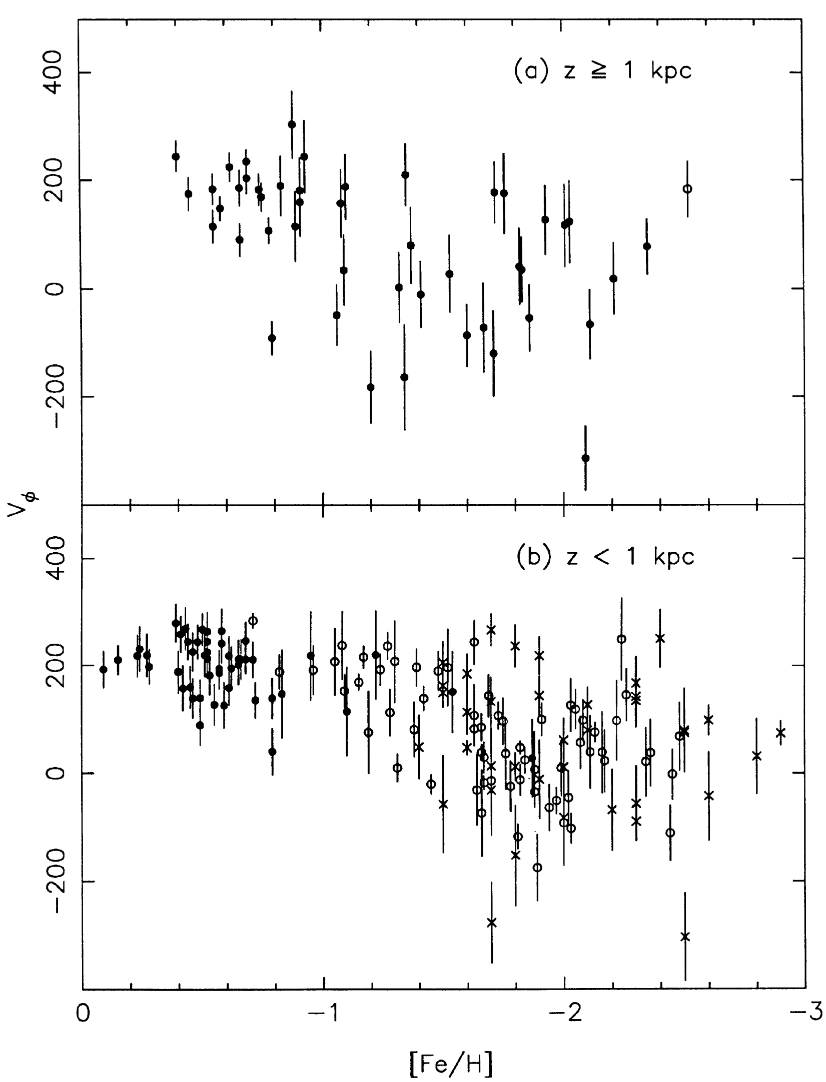

FIG. 6. $\hat{V}_\phi$ vs abundance for the extended sample of giants, shown for $|z|$ heights above and below 1 kpc. Symbols as in Fig. 2. In (a) the giants above 1 kpc are shown. The transition from disk to halo kinematics occurs sharply at $[Fe/H] \approx -1$, contrasting strongly with the giants below 1 kpc in (b), which show evidence for an overlap of disk and halo kinematics in the region $-0.8 > [Fe/H] > -1.6$. The mean $|z|$ height of the stars in (a) is 420 pc and in (b) 1780 pc.

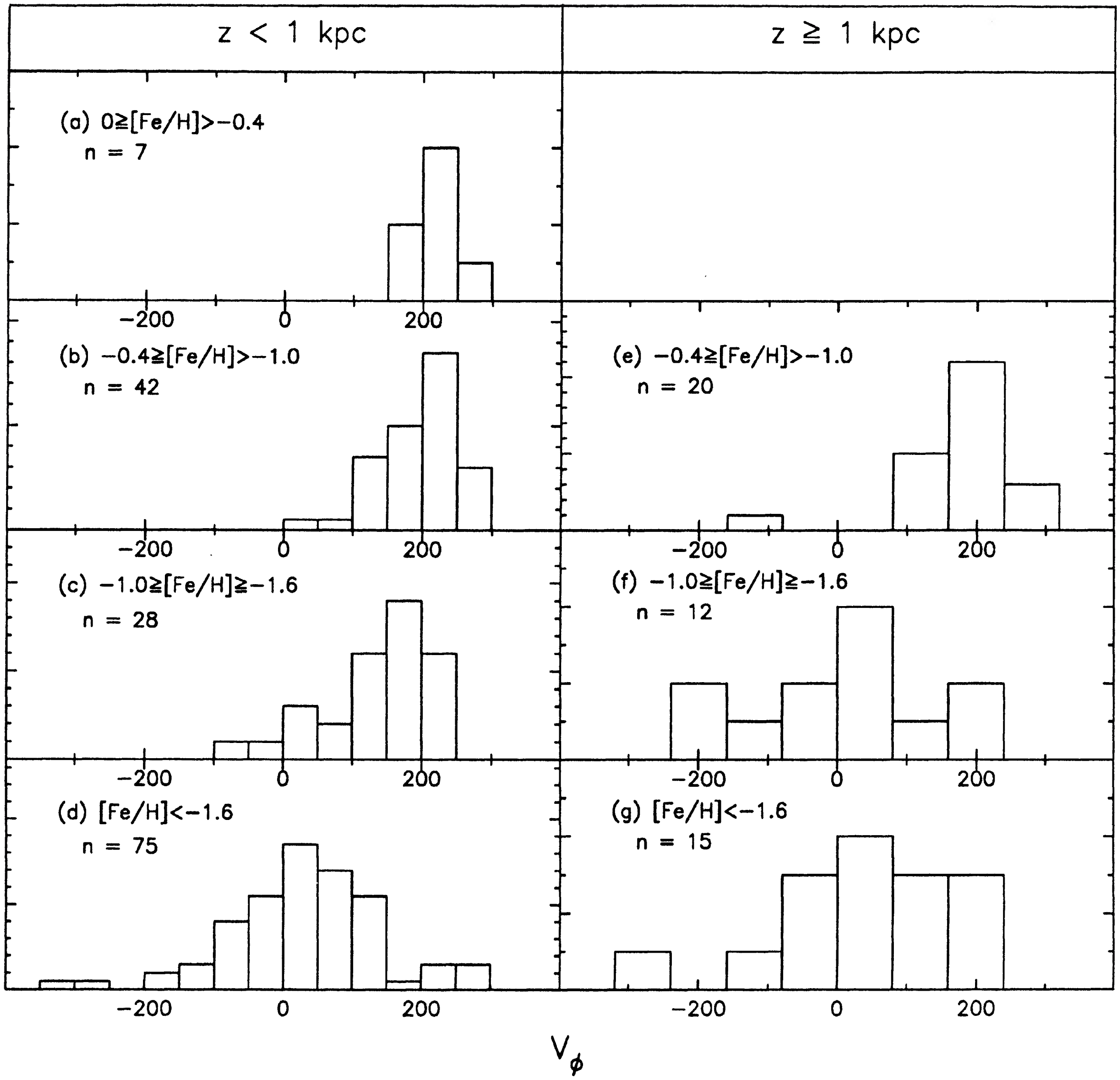

FIG. 7. The velocity histograms for the stars in Fig. 6(a) on the right ($|z| \geqslant 1$ kpc) and 6(b) ($|z| < 1$ kpc) on the left, for various abundance ranges. One tick mark on the *Y* axis corresponds to one star. The histograms for objects above and below 1 kpc are not significantly different at the metal-rich end [(b) and (e)] or the metal-weak end [(d) and (g)]. Compare this to the histograms in (c) and (f) which differ dramatically. (c) shows a dominant component with high rotation and low velocity dispersion, like that seen in (b). The kinematics for these stars are summarized in Table V.

Appendix B for more detail). If the distribution is skewed, we measured the kinematics of the *dominant* component by maximum-likelihood estimation, which is described in more detail below.

1) Stars below 1 kpc

For the histograms of stars with $|z| < 1$ kpc, the following points should be noted:

(a) The metal-strong and metal-weak extremes of the sample have symmetric velocity distributions, as can be seen from Figs. 7(a) and 7(d), respectively. This is consistent with our assumption that the pure disk and halo have Gaussian distributions.

(b) Both histograms for stars with intermediate abundance are asymmetric, as can be seen from Figs. 7(b) and 7(c). The histogram for $-1.0 \geqslant [Fe/H] \geqslant -1.6$ shows the strongest skew. We tested whether this distribution was Gaussian using the Shapiro–Wilk test, a powerful test for Gaussian shape when the sample size is small. The hypothesis of Gaussian shape is rejected at the 97% level. (The test is described in Appendix B.)

(c) For both the asymmetric distributions [Figs. 7(b) and 7(c)], the dominant population has a high rotational velocity and the tails stretch a long way towards low velocity. The modal velocity decreases slightly as [Fe/H] decreases.

Before continuing, we consider again the effect of [Fe/H] errors scattering disk or thick-disk stars to lower abundances. The stars in the extended sample have [Fe/H] errors of 0.2–0.25 dex. We would expect approximately 10 times more stars with $[Fe/H] > -1.0$ than are observed, if abundance errors were the only cause of the apparently metal-weak stars having disk kinematics. A small number of the stars with $-1.0 \geqslant [Fe/H] \geqslant -1.6$ may have large measurement errors, but the majority cannot be explained in this way.

For Figs. 7(b) and 7(c) we used the maximum-likelihood technique to estimate the mean velocity of the dominant component. For a description of the technique, see Appendix B.* We fitted a mixture of two Gaussian components: a "halo" and a "disk" component. We assumed that the halo component had the same distribution as the metal-weak stars of Fig. 7(d), and estimated three parameters: the mean rotation of the disk component, its velocity dispersion, and the proportions of stars with disk and halo kinematics.

For $-0.4 \geqslant [Fe/H] > -1.0$ [Fig. 7(b)] the mean velocity is 202 ± 8 km s^{-1} and the disk accounts for 97% of the data, showing that disk kinematics still predominate in this abundance range. For $-1.0 \geqslant [Fe/H] \geqslant -1.6$ [Fig. 7(c)] the mean velocity of the disk component is 170 ± 15 km s^{-1}; there is a small increase in asymmetric drift as [Fe/H] decreases. Even in this abundance range, the stars with disk kinematics still account for 72% of the data.

2) Stars above 1 kpc

The sample with $|z| \geqslant 1$ kpc is much smaller, but all three distributions shown in Figs. 7(e)–7(g) are roughly symmetric. The gross difference between the kinematics of the stars with $-1.0 \geqslant [Fe/H] \geqslant -1.6$ for different z heights is highlighted by the shape of their velocity histograms. The Shapiro–Wilk test shows that there is no evidence that the stars in this abundance range, with $|z| \geqslant 1$ kpc, are not drawn from a Gaussian distribution.

Kinematical properties for $|z| \geqslant 1$ kpc are as follows:

(a) The metal-strongest stars, with $-0.4 \geqslant [Fe/H] > -1.0$ [Fig. 7(e)], have a mean $V_{\rm rot} = 176 \pm 12$ km s^{-1}, not significantly different from the mean velocity for the dominant component of the corresponding group with $|z| < 1$.

(b) Stars with $-1.0 \geqslant [Fe/H] \geqslant -1.6$ and $|z| \geqslant 1$ kpc [Fig. 7(f)] have a mean velocity of 18 ± 41 km s^{-1}, contrasting strongly with the predominant group of stars in Fig. 7(c) for which $|z| < 1$ kpc and $V_{\rm rot} = 170 \pm 15$.

(c) The metal-weakest stars with $[Fe/H] < -1.6$ in Fig. 7(g) have a mean velocity of 44 ± 34 km s^{-1}, which is not significantly different from the mean velocity (33 ± 11) of stars in this abundance range in Fig. 7(d), which are closer to the plane.

(d) There is no significant difference between the mean rotation of the stars with $-1.0 \geqslant [Fe/H] \geqslant -1.6$ [Fig. 7(f)] and those with $[Fe/H] < -1.6$ [Fig. 7(g)]. Sandage and Fouts (1987, Fig. 26) find a linear relationship between [Fe/H] and $V_{\rm rot}$ for their nearby sample of kinematically selected dwarfs with $|W| > 60$ km s^{-1}; if this were also the case for our data, we would expect the mean rotation of the middle group to be 110 km s^{-1}. Our result (18 ± 41 km s^{-1}) is significantly different at the 95% level, suggesting that the Sandage and Fouts picture is not a good representation of the data above the plane.

We have summarized the kinematics of our enlarged sample in Table V.

3) Two overlapping populations

Is our simple description (of changing contributions of stars with disk and halo kinematics as [Fe/H] decreases) the best description of the data? We note that the data for $|z| < 1$ kpc could also be explained as a continuous decrease in rotational velocity, and a corresponding increase in velocity dispersion as [Fe/H] decreases, as Sandage and Fouts (1987) propose. However, their picture, which we would expect to apply above 1 kpc (because they chose stars with $|W| > 60$ km s^{-1}), does not represent our data for $|z| \geqslant 1$ kpc. We have argued that in the abundance range $-1.0 \geqslant [Fe/H] \geqslant -1.6$, we see two populations overlapping: one with a scale height of approximately 1 kpc, and disk kinematics; and the other with halo kinematics.

If there are two populations overlapping, one might ask why there is a dearth of stars with negative V_ϕ in Fig. 7(c), such as are seen in Fig. 7(d), since we are proposing that the stars with halo kinematics in 7(c) are drawn from the same population as 7(d). If 72% of the 28 stars in Fig. 7(c) have disk kinematics, then we expect only eight of these stars to have halo kinematics; it is possible that we have found no stars with highly retrograde velocities because of small sample statistics. It should also be noted that the abundance distribution of our extended sample in no way reflects the true abundance distribution of the halo; there is a concentration of extremely metal-weak stars due to the selection effects in the NBP and Carney and Latham samples.

4) Measurement of scale height

We have used our enlarged sample to estimate the scale height of the population with disk kinematics by extending the maximum-likelihood procedure described above. The scale height estimate does not come from the z distribution of the stars (as our sample is not spatially complete). However, since the stars have been selected without kinematic bias, it is possible to estimate relative proportions of stars with disk and halo *kinematics* at different z heights. As $|z|$ increases, the proportion of the flattened population with disk kinematics will decrease. This decrease can be modeled as an exponential function, and thus the scale height of the population with disk kinematics is estimated.

We used all stars with $-1.0 \geqslant [Fe/H] \geqslant -1.6$; their z heights range from 30 pc to 4.4 kpc. We assumed, as before, that these stars come from a mixture of populations with disk and halo kinematics, and that the halo parameters could be estimated using the stars with $[Fe/H] < -1.6$. However, this time we assume that the proportion of stars with

TABLE V. Mean rotation (in km s^{-1}) by abundance and z height (for dominant component only if distribution skewed).

	[Fe/H] range			
z height	0 to −0.4	−0.4 to −1.0	−1.0 to −1.6	< −1.6
$\lvert z\rvert < 1$	215 ± 6	202 ± 8 (disk comp.)	170 ± 15 (disk comp.)	37 ± 12
$\lvert z\rvert \geqslant 1$	—	176 ± 12	18 ± 41	44 ± 34

*Note that trimmed estimators were not used for maximum-likelihood estimation.

disk kinematics is $\pi_0 e^{-z/h_z}$, where π_0 is the proportion of disk stars at $z = 0$ and the scale height of the disk population is h_z. (This implicitly assumes that the halo density is uniform over this region in z.) Three parameters are estimated: π_0, h_z, and the mean rotation velocity of the disk component. The effective disk velocity dispersion (which includes the true σ_ϕ, measurement errors, and small contributions from σ_r and σ_θ) is fixed at 45 km s^{-1}: the value given by the previous maximum-likelihood estimate in Sec. VII*b1*. The estimates are:

$$\pi_0 = 0.83 \pm 0.17,$$

$$V_{\rm rot} = 173 \pm 13 \ \ {\rm km\,s^{-1}},$$

$$h_z = 1.4 \pm 0.7 \ \ {\rm kpc}.$$

As we might expect, there is a substantial correlation (-0.55) between estimates of π_0 and h_z.

5) Stars with all three space velocities U, V, W

The extended sample was formed by adding stars from the solar neighborhood. The majority of these stars (93 of 104) have *U*, *V*, and *W* space velocities, unlike our original sample, for which we only have an estimate of V_ϕ. This gives further information on the space distribution of these stars—both an independent check on the scale height h_z, and a measure of the radial scale length h_R.

Figure 8 shows the *W* velocity distribution of the solar neighborhood stars. All of these stars have $z < 1$ kpc, so we would expect to see support for the features identified in Fig. 6(b)—stars with thick disk kinematics predominating for [Fe/H] between -1.0 and -1.6, and stars with halo kinematics predominating for abundances lower than [Fe/H] $= -1.6$. This is indeed what is seen. The stars with [Fe/H] between -1.0 and -1.6 have a relatively low *W* velocity dispersion, as would be expected with a flattened population, and the stars with [Fe/H] < -1.6 have a higher *W* velocity dispersion, as would be expected for the genuine halo stars.

To estimate kinematical parameters for the metal-weak stars with disk kinematics, a maximum-likelihood procedure similar to that used in Sec. VII*b1* was followed. The kinematical data for stars with [Fe/H] between -1.0 and -1.6 was modeled by a mixture of two Gaussian velocity distributions, with the parameters for the halo distribution estimated from the velocities of stars with [Fe/H] < -1.6. The proportion of disk stars was fixed at the value estimated previously (72%), and the maximum-likelihood technique used to estimate the mean velocity and velocity dispersion for the disk component. Solutions were obtained independently for the *U*, *V*, and *W* velocities. Table VI shows the results of this estimation for the three velocity components.

The errors in Table VI in the mean velocity and velocity dispersion are large both because of the small sample in this abundance range (24 stars), and because the errors on individual *U*, *V*, or *W* velocities are quite large (typically 20–30 km s^{-1}, a sizeable proportion of the intrinsic velocity dispersion of the stars). Thus the derived values are not as accurate as we would wish. However, some interesting points can still be deduced from the table.

The mean *V* velocity is (not surprisingly) consistent, within the errors, with the value derived from the larger sample, and the mean *U* and *W* velocities are close to zero, as expected. The *W* velocity dispersion of 40 km s^{-1} is consistent with a scale height of ~1 kpc (Freeman 1987), which is the same, within our quoted errors, as the previous estimate of h_z for these stars (1.4 ± 0.7 kpc). Thus two independent kinematical quantities both show that these stars have a scale height of approximately 1 kpc.

The value of $\sigma_v = 26 \pm 13$ km s^{-1} seems a little small by comparison with the metal-richer stars in our original sample (40 ± 10 km s^{-1}). It is, however, possible to reduce the

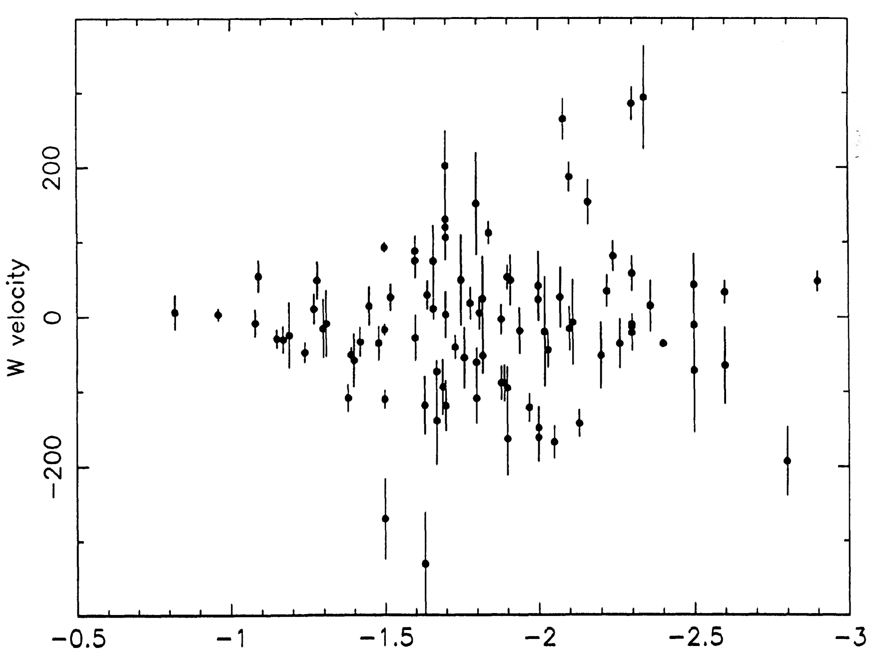

FIG. 8. *W* velocities versus abundance for stars in the extended sample of giants. Note the low velocity dispersion in the range [Fe/H] > -1.6 compared to [Fe/H] < -1.6. All these stars have $|z| < 1$ kpc.

TABLE VI. Mean velocity and velocity dispersion for metal weak stars—disk component.

	Mean velocity ($km\ s^{-1}$)	Velocity dispersion ($km\ s^{-1}$)
U	25 ± 20	65 ± 18
V	-52 ± 14	24 ± 16
W	-10 ± 14	40 ± 13

uncertainty in our estimates of σ_U and σ_V by requiring that their ratio σ_U:$\sigma_V = 2$:$\sqrt{2}$. We would expect this to be a reasonable assumption for these stars, because they are close to the solar radius (so the local rotation curve is flat), and their mean rotation is clearly high. Using this assumption, the allowed ($\pm 1\sigma$) values of (σ_U, σ_V) range from (47, 33) to (56, 40), so we adopt $\sigma_U = 52$ $km\ s^{-1}$ and $\sigma_V = 37$ $km\ s^{-1}$.

We now use Eq. (13) to estimate the radial scale length for these stars as $h_R = 2 \pm 1$ kpc. While we do not attach much weight to this value because of the large errors in the kinematical quantities used to derive it, it agrees quite well with the radial scale length derived for the metal-richer stars in our original sample (3 ± 1 kpc).

c) Comparison with Ratnatunga and Freeman

We will compare our results with a recent survey for distant metal-weak stars. Ratnatunga and Freeman (1989, RF) have published radial velocities and abundances for a group of predominantly metal-weak giants at $l = 272°$, $b = +38°$. These stars are at z distances ranging from 1.5 to 15 kpc, with the metal-weak stars furthest away. The field is far from the tangent point and is not optimally placed for measurement of rotational kinematics, particularly for the more distant, metal-weaker stars. However, it still gives useful information on rotational kinematics away from the plane.

We have calculated* $\hat{V}_\phi$ for their stars. For the metal-weak stars, errors on $\hat{V}_\phi$ due to contamination from other velocity components are some three times higher on average than our errors. However, the RF data show the same abrupt change to halo kinematics around [Fe/H] $= -1.0$ as we see in Fig. 6(a), and so lend support to our claim that the rapidly rotating stars with [Fe/H] < -1.0 are confined to a scale height of approximately 1 kpc.

Using the estimation procedure outlined in Sec. V, we have calculated values of $V_{\rm rot} = -27 \pm 50$ $km\ s^{-1}$, and $\sigma_\phi = 140 \pm 50$ $km\ s^{-1}$ for stars with [Fe/H] < -1.0. We assumed that $(\sigma_r, \sigma_\theta) = (130, 90)$; an increase of 20 $km\ s^{-1}$ in both components decreases the σ_ϕ estimate by 50 $km\ s^{-1}$, so the result is quite sensitive to this assumption.

RF's group of 17 giants with $0.0 >$ [Fe/H] $\geqslant -0.8$ exhibits disk kinematics; we calculate $V_{\rm rot} = 167 \pm 20$ $km\ s^{-1}$, and $\sigma_\phi = 60 \pm 24$ $km\ s^{-1}$, assuming that $(\sigma_r, \sigma_\theta) = (80, 40)$. (This differs slightly from RF's results for the metal-stronger giants because the abundance intervals are not identical.) These stars have mean z height of 3.1 kpc. The assumed value of σ_θ gives a scale height in z of about 1.5 kpc, so the data are consistent with these thick-disk stars being about 2 scale heights from the plane. The large errors are a result of the sensitivity to the assumed σ_r and σ_θ. However, we derive from our sample, within the errors, the same results for $V_{\rm rot}$ and σ_ϕ and confirm their result that the thick disk rotates rapidly.

*The method of analysis differs from RF's: they assumed a velocity ellipsoid constant in *cylindrical* coordinates, while we assume a velocity ellipsoid constant in spherical coordinates.

VIII. DISCUSSION

a) Introduction

In the previous section we established the existence of a group of metal-weak red giants (at the metal-strong end of halo abundances, i.e., [Fe/H] between -1.0 and -1.6) which has disk kinematics:

$$V_{\rm rot} = 173 \pm 13\ \ km\ s^{-1},$$

$$\text{scale height} = 1.4 \pm 0.7\ \ \text{kpc},$$

and predominates at low z heights in this abundance range (around 80% at $z = 0$).

These metal-weak field giants clearly belong to a flattened, rapidly rotating population, although their abundances are in a range traditionally associated with the slowly rotating galactic halo. How then do they fit into the framework of galactic formation and evolution?

We cannot measure the ages of these giants, but we can compare their kinematics with those of traditional halo members: The globular clusters and the local metal-weak RR Lyrae stars. Both were probably formed early in the history of the Galaxy: the globular clusters are believed to have ages in the range 12–18 Gyr (Lee, Demarque, and Zinn 1988; VandenBerg 1988), and while the situation is not as clear for the local RR Lyrae stars, there is no conclusive evidence that there exist metal-weak RR Lyrae stars younger than this.

b) The Globular Clusters

First, let us consider the globular clusters. We have taken the cluster data summarized by Armandroff (1989), and used only the clusters with small errors on his projection factor cos ψ [$\sigma(\cos\psi) < 0.2$]. To make the comparison between the solar neighborhood giants and the clusters as close as possible, we only used clusters with $|z| < 1$ kpc.

We calculated $V_{\rm rot}$ for three abundance bins, using the same methods and assumptions as in Sec. IV. We found that the globular clusters do not exhibit a gradual change from disk to halo kinematics, even when the sample is restricted to $|z| < 1$ kpc: they still show an abrupt change from rapid to slow rotation around [Fe/H] $= -1.0$. Table VII summarizes these results, and gives our own findings for the K giants with $|z| < 1$ kpc for comparison. The behavior of the globular cluster kinematics with abundance is much more like that of our giants with $|z| \geqslant 1$ kpc.

The globular clusters with $-1.0 \geqslant$ [Fe/H] $\geqslant -1.6$ have an average distance of 5.0 kpc from the galactic center: in

TABLE VII. Net rotation (in $km\ s^{-1}$) of globular clusters with $|z| < 1$.

	Globular clusters			Red giants
Abundance range	$V_{\rm rot}$	N	$\langle R \rangle$ kpc	$V_{\rm rot}$
[Fe/H] $\geqslant -1.0$	176 ± 31	6	4.6	205 ± 6
$-1.0 >$ [Fe/H] $\geqslant -1.6$	13 ± 49	7	5.0	170 ± 15
[Fe/H] < -1.6	28 ± 54	4	6.6	37 ± 12

case this causes the difference between K giants and globular clusters, we next consider a sample of local RR Lyrae variables.

c) A Sample of RR Lyraes

We have compiled a sample of 100 local RR Lyraes which have accurate [Fe/H] values [the stars published by Hemenway (1975) whose ΔS values were determined spectroscopically]. Proper motions were taken from the recent survey by Wan, Mao, and Ji (1980); we used stars for which the error in both components of proper motion were less than 0.0120″ per year. Radial velocities were taken from Hawley *et al.* (1986). For consistency with the distance scale used by Armandroff (1989) for the globular clusters, it was assumed that the absolute magnitude of the RR Lyraes is related to [Fe/H] by

$$M_V = 0.20[\mathrm{Fe/H}] + 0.92$$

(Lee, Demarque, and Zinn 1987), and space motions were calculated for the stars.

The two recent calibrations of ΔS in terms of globular cluster [Fe/H] values by Norris (1986) and Zinn (1986) differ by 0.2 dex in zero point; we have adopted the Zinn scale:

$$[\mathrm{Fe/H}] = -0.16\Delta S - 0.41,$$

but note here that the results we produce would not be significantly changed if we had used the Norris scale instead.

We plot V_ϕ vs [Fe/H] for the RR Lyraes with $|z| < 1$ kpc in Fig. 9(a). [We have estimated kinematical quantities for the RR Lyraes using 5% trimmed mean and standard deviation estimators. The errors quoted are not the usual $\sigma/\sqrt{n}$ and $\sigma/\sqrt{2n}$ errors, but calculated specifically for the trimmed estimators, without the assumption of an underlying Gaussian distribution. For derivations, see Welsh and Morrison (1990).]

There is a small group of stars with disk kinematics at the metal-strong end ($\Delta S = 0$ and 1; [Fe/H] from -0.4 to -0.6) for which $\langle V_\sigma \rangle = 184 \pm 15$ km s^{-1}. The stars with $\Delta S = 2$ and 3 ([Fe/H] from -0.7 to -0.9) show only weak evidence of an overlap between disk and halo; and for $\Delta S \geqslant 4$ ([Fe/H] $\leqslant -1.05$) there is no sign of an overlap of disk and halo kinematics, in strong contrast to the G and K giants. For this group $\langle V_\phi \rangle = 64 \pm 16$ km s^{-1}: All these stars have low mean rotation and high σ_ϕ.

Additional evidence that the RR Lyraes have different kinematics from the G and K giants comes from their W velocity distribution. If there was a significant component with disk kinematics and [Fe/H] less than -1.0, then the flattening of the system would be reflected in a low W velocity dispersion for this abundance group. However, examination of Fig. 9(b) suggests that this is not the case. W velocities for the entire sample of RR Lyraes are shown as a function of [Fe/H], and the only significant change in velocity dispersion is for the metal-strong stars with $-0.4 \geqslant [\mathrm{Fe/H}] \geqslant -0.6$.

Table VIII shows values of velocity dispersion for three abundance groups. An F test modified to take the trimming into account (Welsh and Morrison 1990) shows that there is no significant difference* between the velocity dispersions of the groups with $-1.0 \geqslant [\mathrm{Fe/H}] \geqslant -1.6$, and $[\mathrm{Fe/H}] < -1.6$, while there is both a significant difference between the velocity dispersion of the metal-strong group ($-0.4 \geqslant [\mathrm{Fe/H}] \geqslant -0.6$) and the intermediate group (at the 95% level); and between the metal-strong group and the metal-weak group (at the 99.9% level).

Figure 10 illustrates the differences between the RR Lyraes and red giants very clearly. It shows the kinematics of both groups of stars in the abundance range $-1.0 \geqslant [\mathrm{Fe/H}] \geqslant -1.6$. The rotational velocity V_ϕ is plotted against the W velocity. The RR Lyraes (shown at the top) are smoothly distributed in a population with high σ_W and low mean velocity, while the red giants in the lower

*The value of the test statistic in this case was 1.51; in order for the difference to be significant at the 95% level, the test statistic needed to be greater than 4.06; thus there is no evidence in this sample that the two groups have different velocity dispersions.

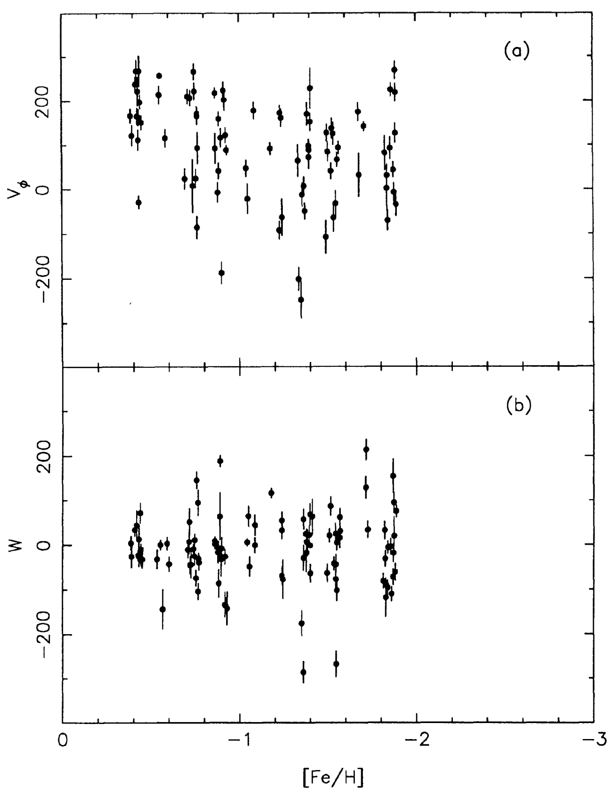

FIG. 9. The azimuthal component of space motion V_ϕ vs abundance for the RR Lyrae sample is shown in (a). A small group of metal-rich objects exhibit disk kinematics. For stars with [Fe/H] below -1.05 there is no sign of an overlap of the disk with the halo. This conclusion is strengthened by the plot of W velocities versus abundance shown in (b). The dispersion in W is uniform for $[\mathrm{Fe/H}] < -1.0$, and only shows a decrease for the metal-rich stars. To display the data more clearly, the [Fe/H] values have been shifted at random by a small amount of up to ± 0.04. Since they are derived from discrete ΔS values, the would have only had ten possible values otherwise.

TABLE VIII. Kinematics for local RR Lyraes.

		All z		$\lvert z\rvert < 1$	
[Fe/H] range	ΔS	σ_W	n	$\langle V_\phi \rangle$	n
-0.4 to -0.6	0,1	27 ± 6	17	184 ± 15	15
-1.05 to -1.6	4,5,6,7	69 ± 17	36	45 ± 24	26
-1.7 to -1.9	8,9	100 ± 17	19	83 ± 27	15

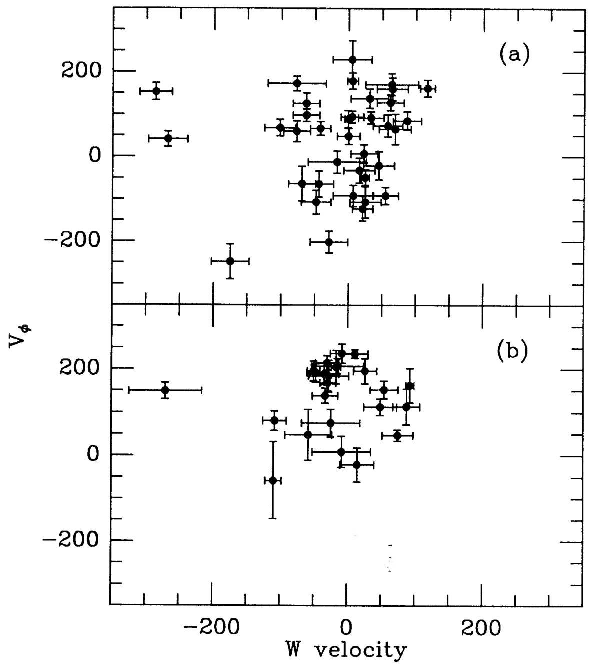

FIG. 10. Plot of V_ϕ vs W velocity for stars with $-1.0 \geqslant [Fe/H] \geqslant -1.6$. In (a) the RR Lyraes are shown, in (b) the red giants from the extended sample with measures of all three space motions. The difference in kinematics between the two groups can be clearly seen; the RR Lyraes in this abundance range have a low mean rotational velocity and high vertical velocity dispersion σ_W, while the red giants show a pronounced clump with high rotational velocity and low σ_W.

graph show a significant clump with high mean rotational velocity and low σ_W.

In summary, our sample of RR Lyraes with $[Fe/H] \leqslant -1.0$ shows no evidence for a flattened rotating subpopulation. The RR Lyrae abundance scale would have to be revised downward by ~ 0.5 dex in order to affect this conclusion. There are some RR Lyraes with low eccentricity orbits, as noted by NBP, and it is possible that a much larger sample would show evidence for a small fraction of the RR Lyraes forming a flattened system. However, such an effect is *far* less significant than that shown by the red giants in this abundance range.

d) Metal-Weak Thick-Disk Stars

We have shown that the globular clusters and the local RR Lyraes do not share the kinematical behavior of the local red giants; there is no evidence for a subpopulation of metal-weak objects with disk kinematics, for either group. If we take the globular clusters and the RR Lyrae stars to be typical halo objects, this suggests that the metal-weak red giants with disk kinematics should not be associated with the halo, but with the disk and thick disk, as originally suggested by NBP. This implies that there is a significant overlap in abundance between the disk and the halo. We suggest that the thick disk should be still characterized as a flattened population with a scale height of ~ 1 kpc and somewhat hotter kinematics than the thin disk, but that it should be thought of as including stars whose abundance is as low as $[Fe/H] = -1.6$.

We now consider the relative numbers of these stars compared to the disk and thick disk. We do not mean to imply that there are three separate populations (disk, thick disk, and metal-weak thick disk); our data do not allow us to discriminate between discrete populations and a continuum. We merely aim to describe the relative numbers of disk stars of different abundance. Although none of the solar neighborhood samples we have used are complete over the abundance range of interest, we can use the fact that they are selected without kinematic bias to estimate the proportion of metal-weak giants with disk and halo *kinematics*; and combine this with estimates of normalization of the old disk, thick disk, and halo from the literature. This will give us a rough idea of the relative numbers at the plane of what we shall term metal-weak thick-disk stars to old disk, thick disk, and halo stars.

If we consider the giants from our sample with [Fe/H] between -1.0 and -1.6, we have shown in Sec. VII*b4* that at $z = 0$, roughly 80% have disk kinematics. Thus, only 20% of giants in this abundance range belong to the halo. Assuming that the field halo giants have a similar abundance distribution to the halo globular clusters (as given in Zinn 1985), roughly half will have abundances between -1.0 and -1.6. Thus the ratio of halo giants with $[Fe/H] < -1.0$ to metal-weak thick-disk giants is 40:80 or 1:2.

Bahcall (1986) estimates the local disk:halo normalization to be about 500:1. Gilmore and Reid (1983) estimate that the thick disk has a normalization of 2% of the local disk, so our rough estimate of the relative numbers of old disk, thick disk, metal-weak thick disk, and halo stars at the plane is

$$500:10:2:1,$$

where the mean abundance for each group is approximately

$$-0.2: -0.6: -1.2: -1.5.$$

Thus it can be seen from these rough estimates that it is reasonable to regard the stars with [Fe/H] between -1.0 and -1.6 and disk kinematics as the metal-weak tail of the thick disk. They only dominate the halo sample because of the extreme rarity of halo stars compared to disk stars, and it is only because our sample was intended to discover halo stars that they were noticed. Any study of the disk would have to contain enormous numbers of metal-strong disk stars in order to contain any metal-weak thick-disk stars.

Our relative proportions are only rough estimates, and depend on the accuracy of both the halo:disk and disk:thick disk normalizations. However, the relatively large number of thick disk stars with $[Fe/H] < -1.0$ ($\sim 20\%$) is in some disagreement with the abundance distributions for the thick disk suggested by Gilmore and Wyse (1985) and Carney, Latham, and Laird (1989: CLL). (The two groups of authors suggest mean abundances of $[Fe/H] = -0.6$ and -0.5, and abundance spreads of $\simeq 0.3$ and 0.2, respectively.) Under either of these hypotheses, one would expect less thick-disk stars with $[Fe/H] < -1.0$ than we observe. However, we note the CLL sample [as shown by Gilmore and Wyse 1989, Fig. 4(b)] does include some stars with $[Fe/H] < -1.0$ and disklike kinematics. Their kinematical selection effects would make these stars less likely to appear in their sample. A more elaborate analysis of both the Gilmore and Wyse (1985) and CLL samples is needed to see whether they show any significant discrepancy with our relatively large fraction of metal-weak thick-disk stars.

e) The Age of the Thick Disk

We have shown in previous sections that there are significant numbers of metal-weak red giants with thick-disk kinematics; in fact at the plane they outnumber "classical" halo stars (i.e., metal-weak stars with high velocity dispersion). We have also shown that the local RR Lyrae variables show very different kinematical behavior—there is no evidence for a dominant population of RR Lyraes with disk kinematics in the abundance range $-1.0 \geqslant [Fe/H] \geqslant -1.6$.

What does this imply about the ages of the metal-weak thick-disk stars? There are globular clusters in this abundance range which have RR Lyrae variables, so we could postulate that these metal-weak thick-disk giants are younger than the globular clusters by several Gyr to explain why the RR Lyrae strip in their horizontal branch is not populated. The core helium burning phase of their evolution would then be spent on the red side of the horizontal branch, rather than in the instability strip as RR Lyraes.

How does this fit in with current estimates of the age of the thick disk? This issue is somewhat contentious at present; we shall briefly review some of the evidence here.

Norris and Green (1989) claimed that the local thick disk is at least 3–6 Gyr younger than the disk globular clusters. They based their claim on the difference in horizontal branch morphology between disk globular clusters such as 47 Tucanae, and old open clusters such as NGC 2243 and Melotte 66, which are ~ 6 Gyr younger. The red horizontal branches of disk globular clusters are significantly bluer than the corresponding feature (the clump stars) in old open clusters. They examined the color distribution of a complete sample of giants at the SGP, and found that the distribution suggested that they are members of the younger clump population. They postulated that the thick disk is the field counterpart of the old open clusters and not the disk globular clusters.

Claims that the thick disk is as old as the disk globular clusters have followed two main lines of reasoning: First, kinematical and other similarities between the populations, and second, turnoff colors of thick-disk field stars.

The "similarity" argument has been most recently used by Armandroff (1989), who derived a mean rotation of the disk globular cluster system of 193 ± 29 km s^{-1}. He noted that the thick disk and disk globular clusters have, within the errors, identical kinematics and abundance distributions, and suggested a similar origin (and implicitly age) for both.

Arguments based on turnoff colors of samples of thick disk stars have been advanced by Wyse and Gilmore (1988) and by CLL. We will consider the data of CLL, as their very accurate abundance measures make it possible to make more sensitive age determinations from turnoff colors. They give a color histogram for the abundance range $-0.35 \geqslant [Fe/H] \geqslant -0.65$, which they associate with thick-disk stars. They note that the turnoff color for NGC 2243 is considerably bluer than the blue edge of their histogram, indicating that it has a younger age than the thick-disk stars. They conclude by comparison with the turnoff color of 47 Tucanae that the thick disk has an age approximately the same as 47 Tucanae.

In order to make the comparison between the field stars and the metal-weaker cluster 47 Tucanae more exact, the $B-V$ turnoff color 47 Tucanae was adjusted redward by 0.02 mag (using the isochrones of VandenBerg and Bell 1985). Two comments are in order here (we are grateful to Dr. J. E. Norris for pointing them out). First, it is more direct to compare the turnoff color for a sample of field stars with similar abundances to 47 Tuc. Second, calculations with the Revised Yale Isochrones (Green, Demarque, and King 1987) show that a difference of 0.25 dex in [Fe/H] changes the turnoff $B-V$ color by 0.05 (assuming an age of 14 Gyr and $Y = 0.25$); in addition, an age difference of 4 Gyr corresponds to a difference in turnoff color of 0.04 (assuming $Z = 0.0035$ and $Y = 0.25$). Thus we see that the use of turnoff color is not very sensitive to changes of only a few Gyr in age, and therefore very large samples are needed to discriminate differences of this size. We note that the Revised Yale Isochrones give a larger correction for the [Fe/H] difference than that used by CLL.

In Fig. 11 we show the $(B-V)_0$ histogram of stars from the CLL sample with $-0.60 \geqslant [Fe/H] \geqslant -0.90$. There are 100 stars in this group, and they have a mean [Fe/H] of -0.75, so are a suitable choice for comparison with the 47 Tucanae color–magnitude diagram. We also show with an arrow the turnoff color of 47 Tucanae: $(B-V)_0 = 0.51$. We derived this value from the color–magnitude diagram of Hesser *et al.* (1987), assuming $E(B-V) = 0.03$ [the two accurate Strömgren photometry determinations of Crawford and Snowden (1975) and Hesser and Philip (1976) agree on this value]. For purposes of comparison, the other arrow is shown 0.05 to the blue, corresponding to an age which is 4 Gyr younger than 47 Tucanae. The corrections derived above indicate that in Fig. 5 of CLL, the turnoff color for 47 Tucanae should be at $B-V = 0.56$, rather than at $B-V = 0.52$. With this revision, their Fig. 5 would look similar to Fig. 11. CLL also remark that the range on [Fe/H] of the stars in their Fig. 5 will "smear out any otherwise sharply defined limit by about ± 0.03 mag." This may be the cause of the stars blueward of the 47 Tucanae turnoff; however, we believe that the sample sizes make it difficult to decide definitively between ages of, say, 10 and 14 Gyr.

In conclusion, we feel that the current evidence (Norris and Green 1989; CLL) does not enable us to conclude without doubt that the thick disk is as old as the globular clusters.

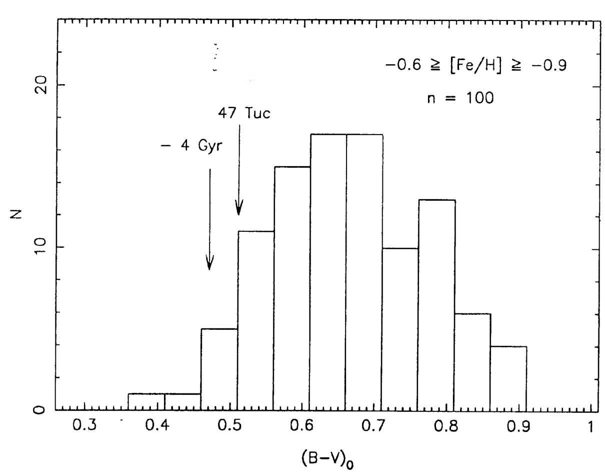

FIG. 11. Plot of $(B-V)_0$ for thick-disk stars in the CLL sample of proper-motion dwarfs, in the abundance range -0.9 to -0.6. This abundance range brackets the metallicity of 47 Tuc. The arrows show the position of the color turnoff of 47 Tuc, and a turnoff 0.05 mag bluer, corresponding to an age 4 Gyr younger.

Hence we will examine our results in the light of both possibilities: a young and an old thick disk.

If the thick disk is significantly younger than the globular clusters, then the natural explanation of our results is that the G and K giants, although metal weak, are younger than the globular clusters and RR Lyrae stars. In this picture, the globular clusters and RR Lyrae stars were formed before the dissipational collapse, and the G and K giants were formed during the collapse. This explains why neither metal-weak globular clusters nor local RR Lyrae stars are seen with the kinematics which are a signature of a dissipational collapse. If so, we have to ask what kind of post-giant branch stars *should* we see if not RR Lyrae stars? Some of the metal-weak thick-disk stars could actually be clump stars in their core He burning phase. It would be interesting to search for metal-weak red horizontal branch stars (like those in NGC 362, M3, or NGC 7006), and examine their kinematics. We predict that a significant number of these stars would be found with disk kinematics, close to the plane.

If the thick disk is coeval with the globular clusters (and, presumably, with the local RR Lyraes as well) then things are more difficult to tie together. If the globular clusters and thick-disk field stars have the same ages, kinematics, and abundance distribution, they are likely to be part of the same population. The lack of metal-weak globular clusters with disk kinematics is unsurprising in the light of the normalization estimate given above: with 20 disk clusters published by Armandroff (1989), the expected number of metal-weak globulars with disk kinematics is approximately 1, which does not strain belief about why the population has not been observed.

The absence of metal-weak RR Lyraes with disk kinematics is harder to understand if the thick disk is as old as the disk globular clusters. Calculations summarized by Taam, Kraft, and Suntzeff (1976) show that it is less probable that a relatively young, massive star will become an RR Lyrae than an older, less massive star. If the metal-weak thick-disk stars are as old as the disk globular clusters, then we would expect to see metal-weak RR Lyraes with disk kinematics. The absence of such stars requires another mechanism which will inhibit formation of RR Lyraes from the metal-weak red giants formed in the dissipational collapse. It is also necessary to explain why this mechanism came into play in the disk at this particular evolutionary stage. This could be another problem to add to the many connected with horizontal branch morphology.

The discussion so far is based on the assumption that the metal-rich and metal-weak stars of the thick disk are coeval. However, the arguments that the thick disk is as old as the globular clusters (CLL, Gilmore and Wyse 1989) apply to the *metal-strong* stars of the thick disk. If these arguments are correct, then the absence of RR Lyrae stars with disk kinematics suggests that our *metal-weak* thick disk stars are in fact younger than the *metal-strong* thick disk. This could readily occur if the galactic halo was not formed during the monolithic collapse of the Galaxy, but came instead from the accretion and subsequent breakup of small metal-weak satellite galaxies over an extended interval of time. For a summary of the accretion picture of the halo, see Freeman (1987). In this picture, the distribution of stars in the early (mainly gaseous) thin disk is thickened by the dynamical effects of satellite accretion (Quinn and Goodman 1986) to form the present *metal-strong* thick disk. The debris of the satellites from this epoch of accretion form the metal-weak halo. We could then interpret the younger *metal-weak* thick-disk stars as the debris of younger metal-weak satellites that were accreted somewhat after the main epoch of halo-forming satellite accretion, following circularization of their orbits by the dynamical friction of the disk. However, it is not clear in this picture why the velocity dispersions and scale heights of the metal-strong and metal-weak thick disks should be so similar.

In summary, if the thick disk is several Gyr younger than the disk globulars, we can simply explain the difference between the kinematics of the metal-weak red giants and the halo tracers as being due to an age difference. If the thick disk is the same age as the disk globulars, it is difficult to explain why we do not see RR Lyraes with similar abundance and kinematics to the metal-weak thick-disk stars. However, since the evidence for the age of the thick disk is not yet conclusive, this may not end up causing any problems.

f) Galactic Formation and Evolution

We have presented evidence for a significant overlap in abundance between halo and disk. What processes during the formation and chemical evolution of the Galaxy would produce disk and halo stars with such disparate kinematics and different ages, but the same abundance?

The model of halo evolution of Hartwick (1976) gives such a mechanism. Hartwick suggested that a significant proportion of enriched gas was lost from halo star-forming sites during its evolution, and that this enriched gas subsequently fell to the disk, dissipated, and formed the first disk stars. The mean abundance of the enriched gas from the halo is the same as the mean abundance of halo stars and clusters, so if this gas was well mixed before forming disk stars, we would expect the first disk stars to have roughly the same abundance as the mean halo abundance, as observed. Chemical evolution models which incorporate such a process include Searle (1979) (after Searle and Zinn 1978), Gilmore and Wyse (1986), and Pagel (1989).

Another possibility is the bulk of the halo was not formed during the collapse of our galaxy, but came from the accretion and subsequent breakup of small satellite galaxies over an extended period of time, as Searle and Zinn (1978) originally suggested (see previous section). If the halo resulted from accretion, the metal-weak thick-disk stars may be original inhabitants of our galaxy—with disk formation starting at a lower abundance than is usually tough ($[Fe/H] \sim -1.5$)—and the halo stars "interlopers." With this picture, the overlap in abundance between disk and halo causes no problems, because the stars originated in different galaxies. Alternatively, the metal-weak thick-disk stars may include debris from accreted satellites whose orbits were circularized by dynamical friction (Quinn and Goodman 1986) before tidal disruption. However, as we have noted in the previous section, the contrasting kinematics of the RR Lyrae stars remain to be explained; the halo forming accretion events must have occurred earlier than the events which formed the metal-weak thick-disk stars.

Our result may also have an effect on studies of galactic chemical evolution. Since studies of detailed abundances of giants in the solar neighborhood are mostly restricted, by considerations of S/N, to very bright and thus nearby stars, studies of chemical evolution, which assume that all stars with $[Fe/H]$ below -1.0 belong to the halo, run the risk of wrongly classifying metal-weak disk stars as halo objects. A study of the relationship between the distribution of elements and kinematics for local stars in the [Fe/H] range from -1 to -1.6 would be interesting; it could give useful information about galactic evolution in the early stages of disk formation, and help decide between the two pictures discussed above. For example, if the halo stars originated outside our galaxy, there could well be differences in abundance patterns between disk and halo stars at the same metallicity.

g) Halo Kinematics

Our result that some metal-weak giants in the solar neighborhood belong to the disk rather than the halo means that previous determinations of the rotation velocity and velocity ellipsoid of the halo should be viewed with caution. Solar neighborhood samples still dominate studies of the galactic halo; in the list of 1200 objects with $[\mathrm{Fe/H}] \leqslant -0.6$ compiled by Norris (1986), 85% of the objects with $[\mathrm{Fe/H}] < -1.0$ have $|z| < 1$ kpc. We have recalculated V_{rot} and the velocity ellipsoid for nonkinematically selected stars from the Norris catalog. We chose stars with $[\mathrm{Fe/H}] \leqslant -1.6$ (to exclude the metal-weak thick-disk stars) and distances $\leqslant 3$ kpc, and calculated values of (σ_r, σ_ϕ, σ_θ) from both radial velocities only (Woolley 1978) and from (U,V,W) space velocities, and averaged the results from the two methods. We find that $V_{\mathrm{rot}} = 25 \pm 15$ km s^{-1} and $(\sigma_r, \sigma_\phi, \sigma_\theta) = (133 \pm 8, 98 \pm 13, 94 \pm 6)$. This is a better representation of the velocity ellipsoid in the solar neighborhood than the previously quoted result of Norris, which was very likely biased by some disk stars. Freeman (1988) used several other methods of constructing a pure halo sample (uncontaminated by metal-weak thick-disk stars). All these methods use kinematic criteria to remove stars on low eccentricity orbits. It is more direct to use [Fe/H] to define the halo, as we have done here. Freeman's results also indicate that the halo has very low rotation.

It is striking how low the rotation of this subsystem of the galaxy is, a fact which needs explaining. Why should there be a chemically well-defined subcomponent, with such low rotation, of an otherwise rapidly rotating Galaxy?

The change in values of the halo velocity ellipsoid has an effect on the inferred shape of the halo. White (1989) gives a relationship between the velocity ellipsoid of a nonrotating population and its flattening. Use of this relationship with the above velocity ellipsoid gives a flattening in the range $b/a = 0.6$–0.7, depending on the assumed potential; this contrasts with the more extreme values of $b/a = 0.3$–0.5 which White derives from a velocity ellipsoid of (σ_R, σ_ϕ, σ_z) = (140, 100, 75) km s^{-1}. Both values disagree with the conclusions of several authors that the halo has a near-spherical shape (see Freeman 1987 and references therein), but both the Hartwick (1987) model and the Wyse and Gilmore (1989) results suggest that a flattening of 0.6 may not be unreasonable, at least for the inner halo.

We note that both the value of σ_ϕ derived from our original sample (102 ± 24) and the solar neighborhood value derived here, are quite close to that predicted by the dynamical model of the galactic halo proposed by Sommer-Larsen (1987), who kindly calculated the expected run of σ_ϕ with distance for our fields. At the tangent point, his model gives $\sigma_\phi = 99$ km s^{-1}.

IX. CONCLUSIONS

We have observed a sample of G and K giants selected spectroscopically for their moderate to extreme metal deficiency in a galactic rotation field. Accurate abundances, distances, and radial velocities have been determined, and the sample has been combined with local giants from the literature, in order to derive the galactocentric rotation and velocity dispersion of the entire range of abundance, from disk to halo.

Objects we identify with the old disk, in the abundance range $0.0 > [\mathrm{Fe/H}] > -0.55$, are rotating rapidly, $V_{\mathrm{rot}} = 214 \pm 10$ km s^{-1}, and have a low azimuthal velocity dispersion, $\sigma_\phi = 40 \pm 11$ km s^{-1}. We have found stars of lower abundance whose kinematical properties are consistent with membership of the thick disk, and whose abundance distribution shows a large overlap with that of the halo. At the metal-rich end of this abundance range, $-0.55 > [\mathrm{Fe/H}] > -0.79$, we derive $V_{\mathrm{rot}} = 185 \pm 10$ km s^{-1}, and $\sigma_\phi = 39 \pm 10$ km s^{-1}. This is only a slight rotational lag on the old disk, confirming the findings of Ratnatunga and Freeman (1989) and Friel (1988). Stars at the metal-weaker end ($-1.0 > [\mathrm{Fe/H}] > -1.6$) have, within the errors, the same rotational velocity ($V_{\mathrm{rot}} = 170 \pm 15$ km s^{-1}), as the metal-richer stars. A comparison of the kinematics of these metal-weaker stars with the kinematics of globular clusters and local RR Lyrae stars lead us to conclude that they are better associated with the disk than with the halo. These stars form the metal-weak tail of the thick disk, as originally suggested by NBP. Thus not all low abundance objects belong to the halo, and it is necessary to extend the conventional description of the abundance distribution of the thick disk (Gilmore and Wyse 1985) to include stars with [Fe/H] as low as -1.6. We have estimated population parameters for these metal-weak thick-disk stars, and find a scale height of 1.4 ± 0.7 kpc, and a normalization roughly equal to that of genuine halo stars, at the plane. Thus they are very rare stars and will be found preferentially in samples biased toward metal-weak objects, which are selected nonkinematically.

For our sample of halo giants, we confirm that the halo has very low rotation, measuring $V_{\mathrm{rot}} = 17 \pm 24$ km s^{-1}, and also measure $\sigma_\phi = 102 \pm 24$ km s^{-1}. In the light of the findings on the metal-weak stars with disk kinematics, the rotational velocity and the velocity ellipsoid for the metal-weak *halo* in the solar neighborhood has been rederived from the large sample of halo objects of Norris (1986), after removal of objects which may be metal-weak thick-disk stars. We derive $V_{\mathrm{rot}} = 25 \pm 15$ km s^{-1} and (σ_r, σ_ϕ, σ_θ) = ($133 \pm 8, 98 \pm 13, 94 \pm 6$) km s^{-1}. This halo velocity ellipsoid is more isotropic than many previous estimates, and thus does not require the extreme values of flattening of the halo which have been inferred previously. Hence information on the shape of the halo from both spatial and kinematical data is now in better accord.

It is a pleasure to thank John Norris for his interest and encouragement during the course of this work; Bruce Carney, Bob Kraft, Alex Rodgers, Leonard Searle, and Jesper Sommer-Larsen for useful discussions and suggestions; Sean Ryan for cheerfully taking some of the observations for us; the UK Schmidt Telescope Unit for providing excellent plate material and Alan Welsh of the Statistics Department, The Faculties, The Australian National University, for his interest in and help with the statistical aspects of the paper. His help has significantly improved our analysis. H.L.M. acknowledges the financial support of a Commonwealth Postgraduate Research Award. C.M.F. acknowledges the financial support of an Australian National University Scholarship and of the Beckwith Trust.

APPENDIX A: DDO CALIBRATIONS

A general description of the DDO intermediate-band photometric system and its applications can be found in McClure (1976) and (1979). There are two different applications of the DDO system, suitable for metal-strong and metal-weak stars. First, Janes (1975) classified disk stars using strength of the blue CN bands as an abundance indicator, and the filters 41, 42, 45, 48 only. Since the CN bands become too weak to be useful for metal-weak stars, the Janes scheme is only applicable to metal-strong stars with $[Fe/H] \gtrsim -0.8$. Second, Norris, Bessell, and Pickles (1985; NBP) used two additional filters (35 and 38) and derived abundances for metal-weaker stars using line-blanketing in the ultraviolet, measured by the 38 filter. In general we use the Janes calibration for stars with $[Fe/H] > -0.8$, and the NBP calibration for stars with $[Fe/H] < -0.8$. However, we have defined a different luminosity classification scheme for metal-weak stars which removes the need for the 35 filter, and we have made some small changes to the NBP abundance calibration. We also examine the region of overlap between the two classification schemes.

a) Giant/Dwarf Classification

We used the formalism defined by Janes (1975) for giant/dwarf classification of metal-strong stars; if the metallicity derived from the Janes δCN index was greater than -0.8, and the DDO colors were on the grid given by Janes, then his absolute magnitude calibration was used. For these stars, we define a giant (luminosity class III) to have $M_V < 1.0$, and an intermediate class (III/IV) to have $1.0 \geqslant M_V > 3.5$.

For metal-weak stars, NBP used a plot of C3538 vs $R-I$ to classify stars in luminosity. Since observations using the 35 filter take significantly longer than those using the other filters, we decided to use a luminosity classification based on the C4548, C4245, and C3842 indices instead; this was equally satisfactory, and required less observing time.

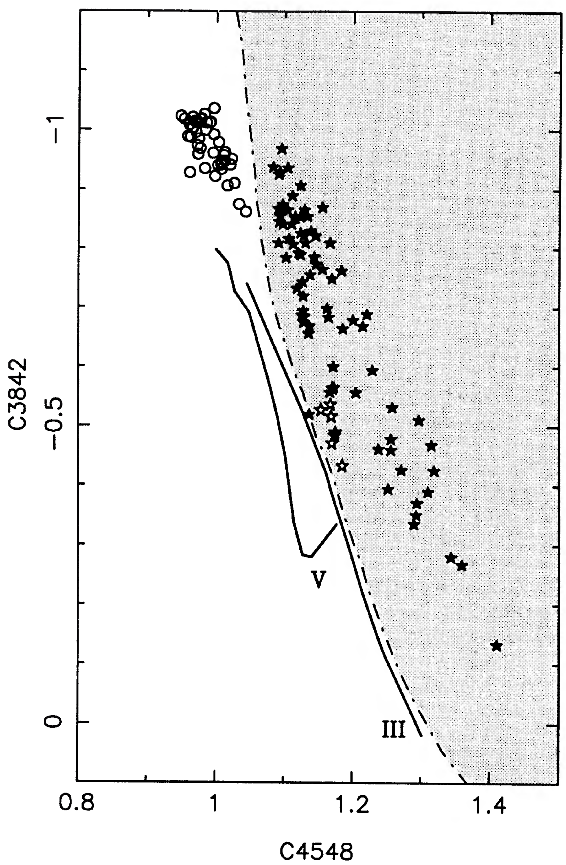

FIG. 13. The C4548–C3842 diagram used in luminosity classification. NBP stars are shown, using the same symbols as in Fig. 1. Metal-weak giants occupy shaded area.

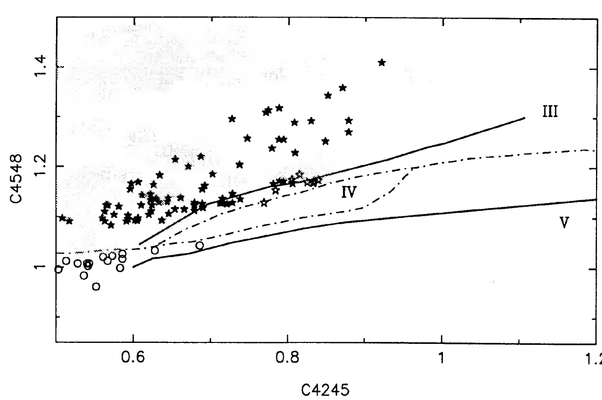

FIG. 12. The C4245–C4548 diagram used in our luminosity classification. The position of dwarfs and giants from the sample of NBP are shown: open circles are dwarfs, filled stars are metal-weak giants ($[Fe/H] < -1.2$), open stars are intermediate metallicity giants ($-0.8 > [Fe/H] \geqslant -1.2$). Also shown are the population I loci for dwarfs, subgiants and giants. Shaded area is occupied by metal-weak giants.

We used DDO photometry of known giants and dwarfs from NBP to set up this classification. Figures 12 and 13 show the regions occupied by metal-weak dwarfs and giants in the C4245–C4548 and C4548–C3842 diagrams. All giants used have $M_V < 1.0$. The mean lines for Population I luminosity classes III and V (taken from McClure and Forrester 1981) are also shown.

In the C4245–C4548 diagram (Fig. 12), it can be seen that there is a clear separation between dwarfs and metal-weak giants for the redder stars (C4245 > 0.7) only. (Note also that the metal-weak dwarfs have similar C4548 colors to the Population I dwarfs.) The C3842 color, however, gives abundance information which makes the distinction between giants and dwarfs much clearer. In the C4548–C3842 plane (Fig. 13), metal-weak giants fall above and to the right of the Population I giant line, and metal-weak dwarfs fall above and to the left of the Population I region.

We classify a star as a giant if it falls in the shaded regions of both Figs. 12 and 13. Subgiants fall in the region marked as IV in Fig. 12; however, the separation between subgiants and dwarfs is less distinct, and we have classified several stars as IV/V when it was not totally clear which class the star should be assigned to. This does not matter in practice, as we are only concerned with identifying the giant stars in our sample.

b) [Fe/H] Measurement

For stars with [Fe/H] greater than -0.8, we used the Janes (1975) δCN calibration. Recent comparisons by Norris and Green (1989—see their Fig. 4, also our Fig. 15) have shown that δCN provides accurate measurements of [Fe/H] down to metallicities of at least -0.7. We adopted the relation

$$[Fe/H] = 4.5\delta CN - 0.2,$$

given by Janes (1975).

For stars with abundances less than -0.8, we used the [Fe/H] calibration of NBP, which uses the C3845 color. C3845 gives a measure of line blanketing in the ultraviolet region. The original calibration of NBP used globular cluster stars only; we have examined its behavior for metal-weak field stars. We collected a sample of stars with abundance determinations either from high-dispersion spectroscopic analysis, from Strömgren photometry, or from the Ca II H and K index A(Ca). Figure 14 shows the external abundance estimate, plotted against the DDO estimate from the NBP calibration. For stars outside the calibration range ([Fe/H] > -0.8), linear extrapolation was used. It can be seen that the 45° line (shown as a dashed line) does not give the best fit to the data: the DDO abundances are systematically too low by about 0.2 dex.

We have therefore corrected the DDO abundances using these data. We calculate [Fe/H] using the method outlined by NBP, and then adjust it using the following formula, obtained from the line of best fit to the data in Fig. 14 (shown as a solid line):

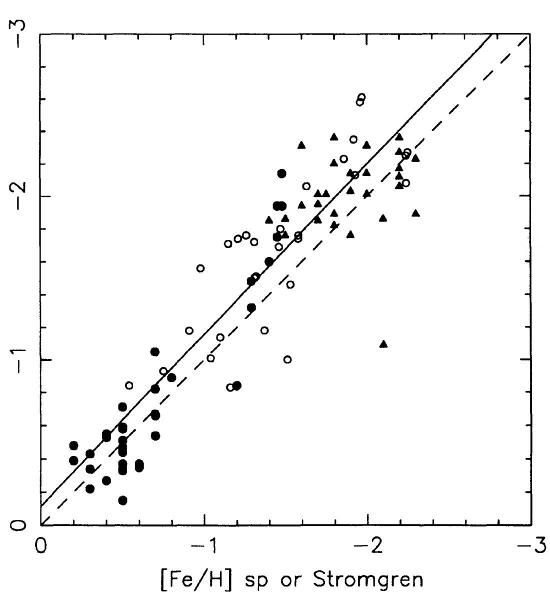

FIG. 14. Comparison of DDO [Fe/H] estimates using the NBP calibration, with other estimates. Filled circles are values from high-dispersion spectroscopic analysis of Cottrell and Sneden (1986), Bond (1980) and Luck, and Bond (1981, 1983). Triangles are values from Strömgren photometry of Eggen (1979) and Bond (1980). Open circles are [Fe/H] values from the Ca II index A(Ca), from Flynn and Morrison (1989). Dashed line is the 1:1 relation; solid line the line of best fit.

$$[Fe/H] = 0.96[Fe/H]_{NBP} + 0.11.$$

In summary, if [Fe/H] from the Janes formalism is greater than -0.8, then the Janes estimate is used. If the revised [Fe/H] from the NBP technique is less than -0.8, we use this; but if both the Janes and revised NBP abundances are within their individual calibration regions (i.e., $[Fe/H]_{Janes} > -0.8$ and $[Fe/H]_{revised\ NBP} < -0.8$), then we average the two estimates.

We estimate errors in [Fe/H] from our two methods to be 0.25 dex. First, considering errors due to the calibration itself, Norris and Green (1989) state that the Janes δ CN abundances are accurate "at the 0.2 dex level." NBP quote a mean absolute difference between their [Fe/H] and that of Eggen and Bond (using Strömgren photometry) of 0.23 dex, which translates to a s.d. of 0.3 dex. This figure includes a contribution from the errors in the Strömgren abundances; if both methods have the same error, it is 0.21 dex. However, our DDO photometric errors are larger than those of NBP; therefore the errors should be a little larger. But Flynn and Morrison (1989) quote a s.d. of 0.3 dex on the difference between A(Ca) and DDO abundances, which shows that this effect must be small. We believe that 0.25 dex thus provides a reasonable estimate of our errors.

c) Absolute Magnitude and Reddening

We used the absolute magnitude calibration of Janes (1975, 1979) for stars with [Fe/H] > -0.8, and that of NBP for stars with [Fe/H] < -0.8. The Janes calibration comes from measurements of M_V for field giants using the Wilson–Bappu effect; the NBP calibration comes from positions of globular cluster giant branches in the M_V, $(B-V)_0$ diagram. Note that for very metal-weak stars ([Fe/H] < -2.3) we do not extrapolate, but use the absolute magnitude of M92, since giant branches of very metal-weak populations are close in M_V, as can be seen from the Revised Yale Isochrones (Green, Demarque, and King 1987). In the metallicity range $-0.6 >$ [Fe/H] > -1.0, the estimates from the two methods were averaged to increase accuracy: this is justified in the next section.

Since all our stars were concentrated in two small areas in the sky, we derived reddenings for these areas by averaging the reddening estimates (found using the method of Janes 1977) for all stars with [Fe/H] > -0.65 in each area.

d) Overlap between the Two Classification Schemes

The calibrations given by Janes and NBP are aimed at different populations, with probably different ages and masses. There is no guarantee that the transition between these two calibrations is a smooth one.

For [Fe/H], it can be seen from Fig. 14 that the *corrected* NBP abundances are accurate for [Fe/H] several tenths of a dex more metal strong than -0.8, where the calibration ends. Figure 15 shows the behavior of the δCN index, applied to the stars with high-dispersion [Fe/H] measurements from Fig. 14. The δCN procedure fails for some of the more metal-weak stars, as they are not on the Janes grid; however, it can be seen that it extrapolates well for the few metal-weak stars on the grid. Therefore, we believe that the transition from disk to halo in metallicity can be measured smoothly, without abrupt discontinuities between the two calibrations.

We have demonstrated that the DDO abundance calibration gives accurate abundances over the entire range of

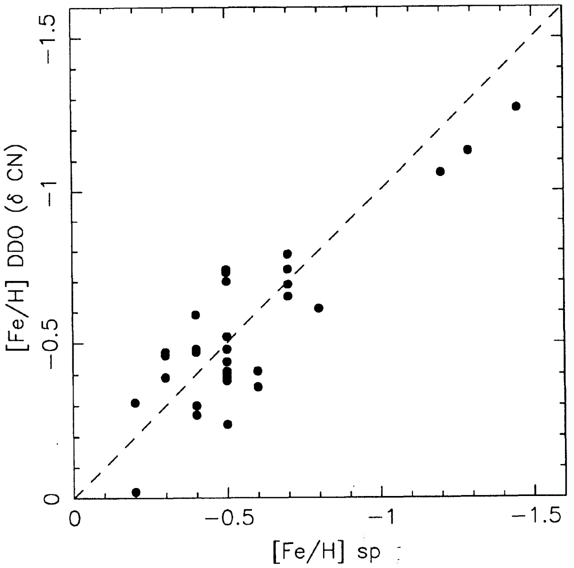

FIG. 15. Comparison of DDO [Fe/H] estimates using the Janes δCN index, for stars with high-dispersion spectroscopic determinations of [Fe/H] as shown in Fig. 13. The dashed line is the 1:1 relation.

[Fe/H] from solar to -2.3; this calibration is tied both to globular cluster giants and to field stars with measures of [Fe/H] from fine analysis. Figure 16 shows the final abundance calibration adopted.

The absolute magnitude calibrations also behave well in the overlap region. Figure 17 shows the difference between the Janes M_V and the NBP M_V for the stars with high-resolution [Fe/H] determinations which have

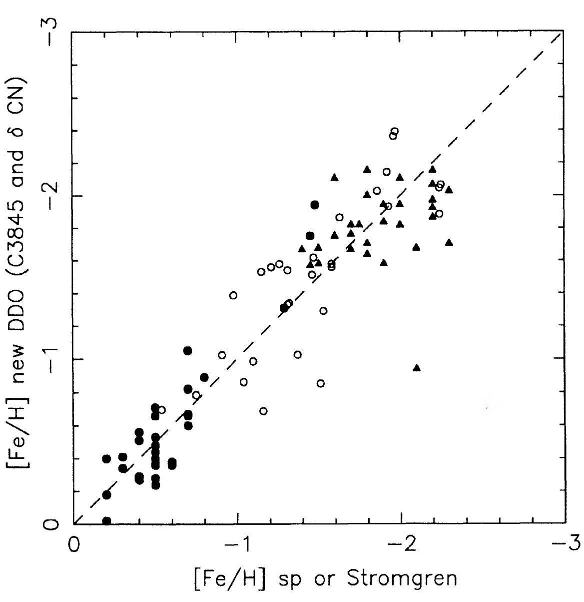

FIG. 16. The final DDO abundance values, using both δCN and C3845, compared with published [Fe/H] values. Symbols are as in Fig. 13; the dashed line is the 1:1 relation.

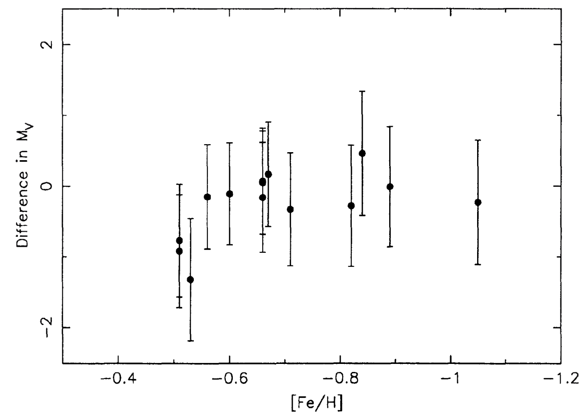

FIG. 17. Difference M_V(Janes) $-$ M_V(NBP) as a function of [Fe/H].

$-1.1 < [Fe/H] < -0.5$. The error bars have been calculated for each absolute magnitude estimate by considering the effect of errors in [Fe/H], and photometric errors in DDO and $B-V$ color, where relevant. In every case but one, the two absolute magnitude determinations are the same, within the errors. Because of this smooth transition, and the large errors in absolute magnitude, we have averaged the Janes and NBP estimates in the region $-1.0 < [Fe/H] < -0.6$, to increase the accuracy of the absolute-magnitude estimate.

e) Iteration

As can be seen from the above description, the DDO classification scheme is complex and inter-related. For example, [Fe/H] influences M_V, and reddening influences everything else. Two iterations are necessary before a consistent abundance and luminosity classification is gained, if the reddening is nonzero.

APPENDIX B: STATISTICAL TECHNIQUES

a) Problems with Outliers

Outliers can adversely affect both estimates of mean velocity and of velocity dispersion. Their effect is particularly bad for velocity dispersion, because observations contribute via their second power, and large velocities will dominate. An example given in Breiman (1973, p. 248) shows the effect of a small number of outliers on a velocity dispersion estimate. He shows that if only one observation out of 20 is affected (by being drawn from a distribution with a larger tail), the error on the classical velocity dispersion estimate* can *triple*.

With the small sample sizes typical of many astronomical investigations, it is almost impossible to detect such subtle variations from Gaussian shape, particularly in the tails of the distribution. However, classical statistical techniques are extremely sensitive to these variations.

Evidence for outliers in the velocity distribution of Galactic halo stars is given by the extreme retrograde stars discussed by Norris and Ryan (1989). Without sample sizes of the order of 1000 stars, we are unable to usefully study the

*$\hat{\sigma} = \sqrt{1/(n-1)\Sigma(x_i - \bar{x})^2}$.

velocity distribution of these retrograde stars; all that is possible is to determine the parameters of the *predominant* distribution, and ensure that our answers are not biased by the rare retrograde stars.

Eddington (1914) proposed using $\Sigma|V|$ rather than ΣV^2 in estimating velocity dispersion, and commented: "This is contrary to the advice of most textbooks, but can be shown to be true." Nowadays it is possible to find textbooks which agree with Eddington! Recent statistical research has identified even better estimators, which make more efficient use of the data, and are not affected by outliers.

b) Trimming the Data

A simple method of protecting estimates from the adverse effect of outliers is to trim one's data. The estimators which replace the classical mean and standard deviation are computationally very simple: one orders the data, removes the highest and lowest 5%, and then calculates the mean and standard deviation with the observations that remain. The choice of how much data to trim (5% here) strikes a balance between throwing away too much data, and risking the effects of outliers on one's data. It is also necessary to renormalize the trimmed standard deviation. (The exact number of observations to be trimmed is found by taking the nearest integer to 0.05 n; if this number is zero, we chose to set it to 1.)

If there are n observations $x_1, x_2, \ldots, x_n$ and $n_{\rm trim}$ are left after trimming, then the trimmed mean is

$$\bar{x}_t = \frac{\Sigma_i x_i}{n_{\rm trim}}, \qquad (14)$$

and the trimmed standard deviation is

$$\sigma_t = \frac{1}{0.789}\sqrt{\frac{1}{n_{\rm trim}-1}\sum_i (x_i - \bar{x}_t)^2}, \qquad (15)$$

where the index i ranges over all observations which have not been trimmed. The factor of 0.789 in Eq. (15) is needed because the removal of the highest and lowest values biases the estimate. It is calculated so that the classical standard deviation and the trimmed standard deviation estimate the same parameter for pure Gaussian data. Details of these estimators can be found in Breiman (1973; p. 241ff), Huber (1981), and Welsh and Morrison (1990).

The trimmed estimates require the user to throw away a small amount of data, but in return they provide safety in estimation. Because of their simplicity, they adapt easily to refinements such as the weighting scheme described in Sec. V. Different choices of the amount to trim may be appropriate for different situations: it is necessary to trade off the loss of precision caused by removing some data points against the loss of precision due to suspected outliers.

To compare the errors of the classical and trimmed estimators, Monte Carlo simulations were made for the two distributions mentioned above: (a) a Gaussian with $\sigma = 1$, and (b) a Gaussian with $\sigma = 1$ which has been contaminated by choosing 5% of the observations from a Gaussian with $\sigma = 5$. The "contaminated" sample is used to illustrate the effects of a distribution with larger tails than a Gaussian: this is the most common deviation from Gaussian shape. Simulations were made for sample sizes ranging from 10 to 1000, and in order to estimate errors with similar precision, the product of the number of simulations and the sample size was kept constant at 100 000.

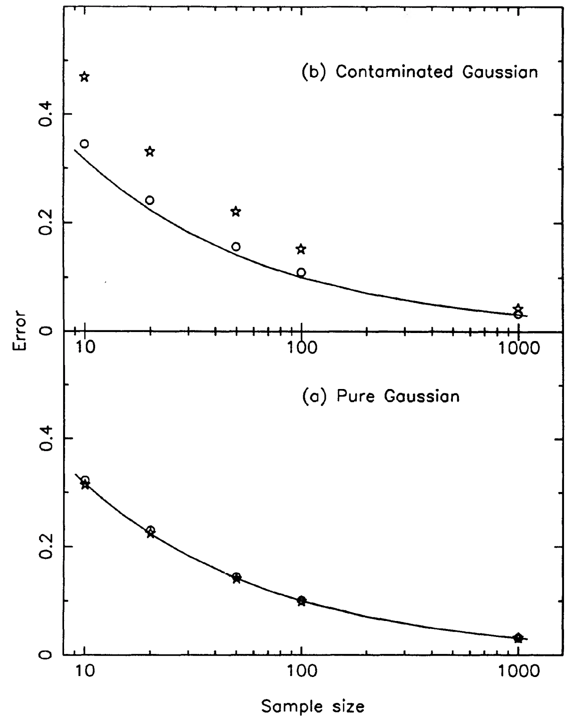

FIG. 18. The error on the mean and 5% trimmed mean, from Monte Carlo simulations. Symbols used are: mean, star; trimmed mean, circle. (a) Data drawn from a Gaussian distribution with $\mu = 0$ and $\sigma = 1$; (b) data drawn from the Gaussian distribution of (a), contaminated by 5% from a Gaussian with $\sigma = 5$. The solid line is the theoretical error on the mean.

The behavior of the trimmed mean can be seen in Fig. 18, which shows the error on the sample mean and the 5% trimmed mean as a function of sample size, for the distributions (a) and (b). The solid line shows the error for the sample mean ($\sigma/\sqrt{n}$) in the case of pure Gaussian data. The trimmed mean has similar errors to the mean for Gaussian data, and performs much better for the contaminated sample.

Figure 19 shows the error on the classical standard deviation and the 5% trimmed standard deviation. The solid line shows the $\sigma/\sqrt{2n}$ error for the standard deviation in the case of a pure Gaussian distribution. The trimmed standard deviation has a slightly larger error for the pure Gaussian case. For the case of a slightly contaminated Gaussian, the errors on the classical standard deviation are much higher, and the trimmed standard deviation is hardly affected; it can be seen that this is the more reliable choice.

c) Maximum Likelihood

This is a general technique of statistical estimation, and has many different applications. Breiman (1973, p. 65) or Kendall and Stuart (1973, p. 38) give introductions to the subject.

We will illustrate the use of the technique using an example: the estimation of velocity dispersion for a group of stars. Let V be the velocity random variable, and $v_1, v_2, \ldots v_n$ the individual measurements of velocity. If we assume that the

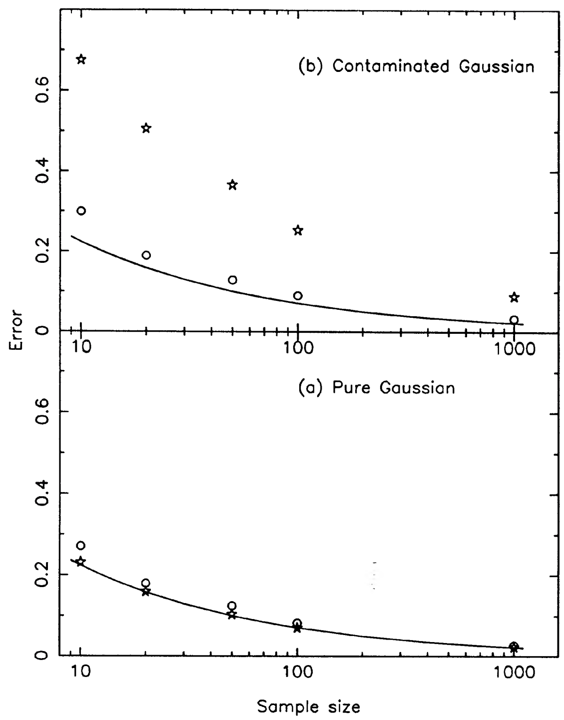

FIG. 19. The error on the standard deviation and 5% trimmed standard deviation estimators. Symbols used are: standard deviation, star; trimmed s.d., circle. Distributions in (a) and (b) the same as in Fig. 16. The solid line is the theoretical approximation to the error on the standard deviation assuming the data are Gaussian.

velocity distribution is Gaussian, with mean zero and velocity dispersion σ, then the probability that the ith velocity is v_i can be written as:

$$P(V=v_i) = \frac{1}{\sigma\sqrt{2\pi}} e^{-v_i^2/2\sigma^2}. \quad (16)$$

Since we know the value of the observed velocity v_i, σ is the only unknown in this equation.

The probability of the whole observed sample of velocities $v_1, v_2, ... v_n$ is just the product of the individual probabilities:

$$l(\sigma) = \prod P(V=v_i) = \left(\frac{1}{\sigma\sqrt{2\pi}}\right)^n e^{-\Sigma v_i^2/2\sigma^2}. \quad (17)$$

We call $l(\sigma)$ the likelihood function.

The maximum-likelihood estimate of σ is found by determining the value of σ which maximizes $l(\sigma)$; equivalently, the value of the parameter σ which would make our observed sample the most probable. In practice, it is simpler to work with the log of the likelihood function, because then the product of Eq. (17) becomes a sum. In simple cases such as the above example, it is possible to derive a formula for the maximum-likelihood estimator of σ by differentiating $l(\sigma)$ and setting the result equal to zero; in more complicated cases the likelihood function is maximized numerically.

Error estimates (and in the case of more than one parameter, estimates of correlation between parameters) are found using the second derivative of the likelihood function, evaluated at the estimated value. In our example,

$$\text{var}(\hat{\sigma}) \simeq -1/l''(\hat{\sigma}) \quad (18)$$

To use the technique, it is necessary to assume a model for the underlying distribution of one's data (often taken to be Gaussian); however, the technique does not provide a direct check of the goodness of fit of this model (for example, whether the Gaussian distribution is the best choice), although it is possible to check this separately in some cases. Thus the technique is model-dependent; and as we have seen in subsection *a* that slightly non-Gaussian distributions can have significant effects on the performance of estimators, this model dependence may be important, and should be recognized.

Also, when a large number of parameters are estimated simultaneously, their values may be correlated: a change in one parameter may be reflected in a compensating change in another. The techniques does estimate these correlations, but they are often not stated in published analyses.

In Sec. VIII*b1*, maximum likelihood was used to fit a mixture of two Gaussian velocity distributions to the data. The mean velocity and velocity dispersion for the halo component (μ_{halo} and σ_{halo}) were assumed known, the mean velocity and velocity dispersion for the disk component (μ_{disk}, σ_{disk}) and the mixture proportion π were estimated. The log likelihood function used was:

$$\log l(\pi, \mu_{\text{disk}}, \sigma_{\text{disk}}) = \sum \log[\pi f_{\text{disk}} + (1-\pi) f_{\text{halo}}], \quad (19)$$

where

$$f_{\text{disk}} = \frac{1}{\sigma_{\text{disk}}\sqrt{2\pi}} e^{-(v_i-\mu_{\text{disk}})^2/2\sigma^2_{\text{disk}}}, \quad (20)$$

$$f_{\text{halo}} = \frac{1}{\sigma_{\text{halo}}\sqrt{2\pi}} e^{-(v_i-\mu_{\text{halo}})^2/2\sigma^2_{\text{halo}}}, \quad (21)$$

and the v_i are the velocity observations.

In Sec. VII*b4*, this procedure was extended to estimate the scale height of the disk component from the change in kinematics with z height. The log likelihood function was:

$$log\, l(\pi_0, \mu_{disk}, h_z) = \sum log[\pi f_{disk} + (1-\pi) f_{halo}], \quad (22)$$

where f_{disk} and f_{halo} have the same functional form as before, and

$$\pi = \pi_0 e^{-z/h_z}, \quad (23)$$

with μ_{halo}, σ_{halo}, and σ_{disk} now fixed.

d) Testing for Gaussian Shape

The Kolmogorov–Smirnov test is frequently used when testing for Gaussian shape. It is a good general test for deciding whether two sets of data are drawn from the same distribution, but there are more sensitive tests available for the special case of checking for Gaussian shape.

A comprehensive review of tests of goodness of fit is given by D'Agostino and Stephens (1986); they have a useful chapter on graphical techniques. They comment about testing for Gaussian shape: "...the Kolmogorov–Smirnov test is only a historical curiosity. It should never be used."

One of the tests they recommend for small sample sizes is the Shapiro–Wilk test. The test is based on the use of probability plots, where the sample cumulative distribution function is plotted with a vertical scale such that Gaussian data form a straight line. The slope of this line gives an estimate of

σ for the Gaussian distribution. The Shapiro–Wilk test compares this estimate with the sample standard deviation; if the two estimates agree, the data come from a Gaussian distribution.

This test is much more powerful than the Kolmogorov–Smirnov test. Detailed instructions for performing the test, and significance levels, can be found in Shapiro and Wilk (1965). It is used for sample sizes of 50 and below; extensions to larger sample sizes can be found in D'Agostino (1971) and Shapiro and Francia (1972).

REFERENCES

Armandroff, T. E. (1989). Astron. J. **97**, 375.
Bahcall, J. N. (1986). Annu. Rev. Astron. Astrophys. **24**, 577.
Bessell, M. S. (1988). Astron. Astrophys. (submitted).
Bond, H. E. (1980). Astrophys. J. Suppl. **44**, 517.
Breiman, L. (1973). *Statistics with a View toward Applications* (Houghton Mifflin, Boston).
Carney, B. W., and Latham, D. W. (1986). Astron. J. **92**, 60.
Carney, B. W., Latham, D. W., and Laird, J. B. (1989). Astron. J. **97**, 423 (CLL).
Cottrell, P. L., and Sneden, C. (1986). Astron. Astrophys. **161**, 314.
Crawford, D. L., and Snowden, M. S. (1975). Publ. Astron. Soc. Pac. **87**, 561.
D'Agostino, R. B. (1971). Biometrika **58**, p. 341.
D'Agostino, R. B., and Stephens, M. A. (1986). *Goodness of Fit Techniques* (Marcel Dekker, New York).
Delhaye, J. (1965). In *Galactic Structure*, edited by A. Blaauw and M. Schmidt (Chicago University, Chicago).
Eddington, A. S. (1914). *Stellar Movements and the Structure of the Universe* (Macmillan, London), p. 147.
Eggen, O. J. (1979). Astrophys. J. **229**, 158.
Flynn, C., and Morrison, H. L. (1990) Astron. J. **100**, 1181.
Freeman, K. C. (1987). Annu. Rev. Astron. Astrophys. **25**, 603.
Freeman, K. C. (1988). In *The Outer Galaxy*, edited by L. Blitz, and F. J. Lockman (Springer, Berlin).
Frenk, C. S., and White, S. D. M. (1980). Mon. Not. R. Astron. Soc. **193**, 295.
Friel, E. D. (1988). Astron. J. **95**, 1727.
Friel, E. D. (1989). Private communication.
Fuchs, B., and Wielen, R. (1987). In *The Galaxy*, Nato Advanced Study Institute, edited by G. Gilmore and R. Carswell (Reidel, Dordrecht).
Gilmore, G., and Reid, N. (1982). Mon. Not. R. Astron. Soc. **202**, 1025.
Gilmore, G., and Wyse, R. F. G., (1985). Astron. J. **90**, 2015.
Gilmore, G., and Wyse, R. F. G. (1986). Nature **322**, 806.
Gilmore, G., and Wyse, R. F. G., (1989). Preprint.
Graham, J. A. (1982). Publ. Astron. Soc. Pac. **94**, 244.
Green, E. M., Demarque, P., and King, C. (1987). *The Revised Yale Isochrones and Luminosity Functions* (Yale University, New Haven).
Hartwick, F. D. A. (1976). Astrophys. J. **209**, 418.
Hartwick, F. D. A. (1987). In *The Galaxy*, Nato Advanced Study Institute, edited by G. Gilmore and R. Carswell (Reidel, Dordrecht).
Hawley, S. L., Jeffreys, W. H., Barnes, T. G., and Wan, L. (1986). Astrophys. J. **302**, 626.
Hemenway, M. K. (1975). Astron. J. **80**, 199.
Hesser, J. E., Harris, W. E., Vandenberg, D. A., Allwright, J. W. B., Shott, P., and Stetson, P. B. (1987). Publ. Astron. Soc. Pac. **99**, 739.
Hesser, J. E., and Philip, A. G. D. (1976). Publ. Astron. Soc. Pac. **88**, 89.
Huber, P. J. (1981). *Robust Statistics* (Wiley, New York).
Janes, K. A. (1975). Astrophys. J. Suppl. **29**, 161.
Janes, K. A. (1977). Publ. Astron. Soc. Pac. **89**, 576.
Janes, K. A. (1979). Astrophys. J. Suppl. **39**, 135.
Kendall, M., and Stuart, A. (1979). *The Advanced Theory of Statistics*, Volume 2, *Inference and Relationship* (Macmillan, New York).
Landolt, A. U. (1983). Astron. J. **88**, 439.
Lee, Y.-W., Demarque, P., and Zinn, R. (1987). In *The Second Conference on Faint Blue Stars*, IAU Colloquium No. 95, edited by A. G. D. Philip, D. S. Hayes, and J. W. Leibert (Davis, Schenectady), p. 137.
Lee, Y.-W., Demarque, P., and Zinn, R. (1988). In *The Calibration of Stellar Ages*, edited by A. G. D. Philip (Davis, Schenectady).
Lewis, J. R., and Freeman, K. C. (1989). Astron. J. **97**, 139.
Luck, R. E., and Bond, H. E. (1981). Astrophys. J. **244**, 919.
Luck, R. E., and Bond, H. E. (1983). Astrophys J. **271**, L75.
McClure, R. D. (1976). Astron. J. **81**, 182.
McClure, R. D. (1979). In Dudley Obs. Rept. No. 14, *Problems of Calibration of Multicolor Photometric Systems*, edited by A. G. D. Philip, p. 83.
McClure, R. D., and Forrester, W. T. (1981). Publ. Dom. Astrophys. Obs. Victoria, **15**, 439.
Menzies, J. W., Banfield, R. M., and Laing, J. D. (1980). S. Afr. Astron. Obs. Circ. **1**, 149.
Morrison, H. L. (1990). In preparation.
Norris, J. (1986). Astrophys. J. Suppl. **61**, 667.
Norris, J. (1987). Astrophys. J. **314**, L39.
Norris, J., Bessell, M. S., and Pickles, A. J. (1985). Astrophys. J. Suppl. **58**, 463 (NBP).
Norris, J. E., and Green, E. M. (1989). Astrophys. J. **337**, 272.
Norris, J. E., and Ryan, S. G. (1989). Astrophys. J. **336**, L17.
Oort, J. H. (1965). In *Galactic Structure*, edited by A. Blaauw and M. Schmidt (Chicago University, Chicago).
Pagel, B. E. J. (1989). Rev. Mex. Astron. Astrofix **18**, 161.
Quinn, P. J., and Goodman J. (1986). Astrophys. J. **309**, 472.
Ratnatunga, K. U., and Freeman, K. C. (1989). Astrophys. J. **339**, 126 (RF).
Sandage, A., and Fouts, G. (1987). Astron. J. **93**, 74.
Searle, L. (1979). In *Les Elements et les Isotopes en l'Universe*, Proceedings of the 22nd International Colloquium of Astrophysics, Liege.
Searle, L., and Zinn, R. (1978). Astrophys. J. **225**, 357.
Shapiro, S. S., and Francia, R. S. (1972). J. Am. Stat. Assoc. **67**, 215.
Shapiro, S. S., and Wilk, M. B. (1965). Biometrika **52**, 591.
Sommer-Larsen, J. (1987). Mon. Not. R. Astron. Soc. **282**, 21P.
Stapinski, T. E., Rodgers, A. W., and Ellis, M. J. (1981). Publ. Astron. Soc. Pac. **93**, 242.
Stock, J. (1984). Rev. Mex. Astron. Astrofis. **9**, 77.
Stock, J., MacConnell, D. J., Osborn, W., and Alvarez, H. (1984). Astron. J. **89**, 1897.
Strömgren, B. (1987). In *The Galaxy*, Nato Advanced Study Institute, edited by G. Gilmore and R. Carswell (Reidel, Dordrecht).
Taam, R. E., Kraft, R. P., and Suntzeff, N. (1976). Astrophys. J. **207**, 201.
Taylor, B. J. (1982). Vistas Astron. **26**, 253.
VandenBerg, D. (1988). In *Globular Cluster Systems in Galaxies*, edited by J. Grindley and A. G. D. Philip (Reidel, Dordrecht).
VandenBerg, D., and Bell, R. A. (1985). Astrophys. J. Suppl. **58**, 561.
van der Kruit, P. C. (1988). Preprint.
Wan, L., Mao, Y.-Q., and Ji, D.-S. (1980). Ann. Shanghai Obs. **2**, 1.
Webbink, R. F. (1981). Astrophys. J. Suppl. **45**, 259.
Welsh, A. H., and Morrison, H. L. (1990). J. Am. Stat. Assoc. (in press).
White, S. D. M. (1989). Mon. Not. R. Astron. Soc. **237**, 41P.
Woolley, R. (1978). Mon. Not. R. Astron. Soc. **184**, 311.
Wyse, R. F. G., and Gilmore, G. (1988). Astron. J. **95**, 1404.
Wyse, R. F. G., and Gilmore, G. (1989). Comments on Astrophys. **13**, 135.
Yoshii, Y., and Saio, H. (1979). Publ. Astron. Soc. Jpn. **31**, 339.
Zinn, R. (1985). Astrophys. J. **293**, 424.
Zinn, R. (1986). In *Stellar Populations*, edited by C. A. Norman, A. Renzini, and M. Tosi (Cambridge University, Cambridge).
Zinn, R., and West, M. J. (1984). Astrophys. J. Suppl. **55**, 45.